Thixotropic injectable hydrogel using a polyampholyte and nanosilicate prepared directly after cryopreservation

Minkle Jain, Kazuaki Matsumura*

School of Materials Science, Japan Advanced Institute of Science and Technology, 1-1 Asahidai, Nomi, Ishikawa 923-1292, Japan

*Correspondence to: Associate Professor Kazuaki Matsumura,

E-mail: mkazuaki@jaist.ac.jp

Abstract

Success of tissue engineering applications in regenerative medicine requires the preservation of tissue-engineered products at a low temperature. This can be successfully achieved by the use of cryoprotective agent (CPA). In this study, we formulated a unique injectable hydrogel for the purpose of cell delivery after cryopreservation by using polyampholyte CPA. The polyampholyte showed excellent post-thaw cell survival, and after thawing, the polymeric CPA did not have to be removed because of its low cytotoxicity. The polyampholyte could be transformed into a hydrogel by mixing with nanosilicates. Previously, nanosilicates were used to improve mechanical properties, but this is the first report of the use of a nanosilicate together with CPA to formulate hydrogels. Inclusion of the nanosilicate led to the formation of thixotropic hydrogels, which can be injected using fine needles. These gels with tunable mechanical properties can be injected into defect sites to form scaffolds for cell growth and tissue repair, and they do not require any separate seeding of cells before injection, thus eliminating the need for cell harvesting and cell maintenance. This is a distinct system in which cells can be cryopreserved until before usage; when required, the cells in the polyampholyte can be revived to their original state and the thixotropic hydrogel can be

formed. The combination of thixotropy and cytocompatibility of the gels could enable a wide range of biomedical applications such as cell delivery and orthopedic repair.

Keywords: thixotropy, polyampholyte, cryopreservation, nanocomposite, injectable hydrogel

1. Introduction

Structures existing in nature usually inspire for biomaterial construction. Designing of such biomaterials for tissue engineering applications requires a detailed understanding of polymers, cells, and nanostructures [1]. To recapitulate these features, various nanoceramics, such as synthetic silicates [2], nano-hydroxyapatite [3-6] and bioactive glass [7-9] have been used. Additionally, various novel microscale technologies have been developed to create polymeric-based structures with nanofillers to provide architecture and materials similar to those in nature [10]. Nanocomposite hydrogels have attractive features, such as highly hydrated 3D polymeric networks with nanoparticles and cytocompatibility. The interaction of nanoparticles with polymers may be covalent [11-13] or physical [14-16], and the design of such systems can give rise to numerous unique and useful combinations that provide distinct attributes such as mechanical improvement, cell adhesiveness and degradation tunability.

Synthetic nanoclays comprised of hectorites, such as laponite, have attracted much interest [17]. Laponite has a disc-like shape, with a diameter of about 25–30 nm, and a thickness of 1 nm [18-20], where the disc has an anisotropic distribution of charges. A negative charge particularly exists on the surface, and the charge on the rim is pH-dependent, with a negative charge at high pH and positive charge at low pH [21,22]. This unusual charge distribution plays a critical role in determining the interactions of laponite with polymers, which are not simple and vary according to the type [23], molecular weight [24], and charge of the polymer [25]. One interesting property of laponite is cytocompatibility. In a previous study, a bioinert polyethylene oxide hydrogel was shown to acquire high cell adhesion through incorporation of laponite [15]. These special properties made laponite an ideal candidate to be used as a filler in the current study.

Various studies have shown that physical interaction of natural and synthetic polymers with synthetic silicates leads to the formation of physically cross-linked structures [11,14,26]. Polyampholytes are a special class of polymers in which cationic and anionic sites are randomly distributed along the polymer backbone [27,28]. In these polymers, it may be possible that one charged species surmounts the others or one of the charged species is dominant in a narrow pH range. Typically, polyampholytes carry net charges that can be tuned by changes in the pH and ionic strength of the system under study. Polyampholytes have found applications in various biomedical fields, such as antibiofouling [29], cryoprotection [30-35], and protein aggregation inhibition [36]. Carboxylated poly-L-lysine (COOH-PLL) is a polyampholyte and was reported to possess excellent cryopreservation ability when present at an appropriate ratio of amino to carboxyl groups [37]. The application of low-temperature preservation has revolutionized biotechnology, as both prokaryotic and eukaryotic cells can be cryopreserved at temperatures of -200°C. In a previous study, we developed a polyampholyte hydrogel having cryoprotective properties via click chemistry [38].

Previously, various studies used laponite as a nanofiller to improve mechanical properties; however, to our knowledge, no study has used a cryoprotective polymer together with laponite. Inclusion of the cryoprotective polymer enables cells to be cryopreserved for a long time such that they can be revived to their original state, whenever required.

In this study, we formulated a novel injectable hydrogel for the purpose of cell delivery by using polyampholyte CPA (Figure1). This is a unique system in which cells can be preserved until before usage and where after thawing, the cells in the hydrogel can be injected easily, without the need to wash out the CPA.

2. Materials and Methods

2.1 Polyampholyte preparation

COOH-PLL was prepared as reported previously in the literature [37]. To synthesize COOH-PLL, 25% (w/w) ε-poly-L-lysine (PLL) aqueous solution was purchased from JNC Corp., (Tokyo, Japan) and mixed with succinic anhydride (SA) (Wako Pure Chem. Ind. Ltd., Osaka, Japan) at 0%–90% molar ratios (SA/PLL amino groups) and reacted at 50°C for 1 h to convert amino groups into carboxyl groups. Thus, carboxyl groups were introduced into PLL by treatment with SA, which reacts with amino groups as shown in Scheme 1. The ratio of carboxylation was well controlled by reaction with SA [35]. The succination ratio in this study was controlled to approximately 50, 65, and 90 mol%. The amount of amino groups in polyampholytes was determined by ^{1}H-nuclear magnetic resonance (NMR) (Avance III 400, Bruker Biospin Inc., Switzerland) and the 2,4,6-trinitrobenzenesulfonate (TNBS) method [39]. The ratio of carboxylation is shown in parentheses, e.g., PLL (0.65) indicates that 65% of the α-amino groups have been converted into carboxyl groups by SA addition.

2.2 Zeta potential measurement

Zeta potentials of PLL (0.5), PLL (0.65), and PLL (0.9) were determined by laser Doppler electrophoresis in a Zetasizer 3000 system (Malvern instruments, Worcestershire, UK) at various pH values. Solutions were prepared in water and the concentration for the measurement was 0.1%. The pH was adjusted using 1M HCl and NaOH solutions.

2.3 Nanocomposite formulation

Stock solutions with varying concentrations of COOH-PLL and laponite (XLG) with a chemical composition of $Na^{+0.7}[(Mg_{5.5}Li_{0.3})Si_8O_{20}(OH)_4]^{-0.7}$ (BYK-Chemie GmbH, Wesel, Germany) were prepared in milli-Q water, which was used to retard gelation and allow complete dissolution of laponite particles prior to gelling. Nanocomposites were allowed to settle at room temperature until a clear gel was formed. Nanocomposite compositions were

prepared by mixing the COOH-PLL and laponite stock and then stirring this mixture vigorously for 15 minutes to achieve the required polymer concentration and laponite loading. Prior to all analyses, all nanocomposites were allowed to settle for 30 minutes after preparation. Nanocomposites are coded as $N_xP(y)_z$ (where x, y, and z represent the solid weight percentage of laponite, the succination percentage, and the solid weight percentage of the polymer, respectively).

2.4 ATR-FTIR

The formation of nanocomposites was characterized by attenuated total reflectance Fourier transform infrared (ATR–FTIR). The lyophilized nanocomposite was mounted on ZnSe crystal on the single-reflection ATR accessory (JASCO ATR PRO450-S), and spectra were obtained using a JASCO FT/IR-4200 system.

2.5 X-ray diffraction (XRD) measurements

XRD measurements were performed using a Miniflex600 diffractometer (Rigaku, Japan) with Cu Kα radiation of 1.54 Å. Diffraction patterns were collected from 2Θ= 2° to 40° with increments of 0.01˚. All collected data were normalized to the same baseline for comparison of the final results. Samples were dried and stored in a desiccator before each measurement.

2.6 Rheological analysis

Dynamic mechanical analysis was performed using the Rheosol-G5000 rheometer (UBM Co., Ltd., Kyoto, Japan). Moreover, a cone plate (39.99 mm diameter) with a gap height of 60 μm and a cone angle of 1.994° was used. All analyses were performed at 37°C, and mineral oil was placed around the circumference to prevent evaporation of water from the nanocomposite to minimize the effects of any shear associated with sample loading. All experiments were performed 10 minutes after loading. Frequency sweep experiments between 0.628 and 62.8 rad・s^{-1} were performed at fixed strain amplitude of 0.967% to measure the storage modulus

(G′) and loss modulus (G″). This strain amplitude was selected because under this strain, our materials show linear viscoelastic behavior. All experiments were performed in triplicate to check the reproducibility of the data.

To evaluate the thixotropy of the nanocomposites, a hysteresis loop experiment was performed by subjecting the hydrogel to a shear rate of 11 s^{-1} for 10 s.

2.7 Cryopreservation protocol and determination of cell survival

COOH-PLL cryopreservation solutions were prepared as follows: PLL (0.65) was dissolved in Dulbecco's modified Eagle medium (DMEM) without fetal bovine serum (FBS) at a concentration of 7.5%, 10%, or 20% (w/v) and the pH was adjusted to 7.4 by HCl or NaOH. Osmotic pressure was adjusted by addition of 10 w% NaCl aqueous solution to a physiological value of 300 mOsm/kg, determined using an Osmometer 5520 (Wescor, Inc., UT, USA). MC3T3-E1 cells were suspended in 1 mL of COOH-PLL cryopreservation solution at a density of 1×10^6 cells/mL in cryovials and stored in a -80˚C freezer for 24 hours. To evaluate cell viability, individual vials were immersed in a water bath at 37°C, and the thawed cells were diluted 10-fold in DMEM. After centrifugation, the supernatant was removed and the cells were resuspended in 5 mL of medium. All the cells were counted using a hemocytometer, and the trypan blue staining method was used to determine cell viability [40,41]. The reported values are the ratios of living cells to total cells.

2.8 Cell adhesion and viability

Biomedical applicability of the nanocomposites was determined by seeding MC3T3-E1 mouse preosteoblasts on the nanocomposite surface. Cell adhesion was determined by seeding 1.0×10^4 cells on $N_3P(65)_{1.5}$, $N_6P(65)_{1.5}$, and on a tissue culture plate (TCP) as a control. At 7 days post seeding, cells were fixed using 3.7% formaldehyde solution and the cell cytoskeleton was labeled with Alexa Flour 488 phalloidin fluorescent dye (Life Technologies, Carlsbad, CA, USA). Cell growth curves on these hydrogels were obtained using Cell

Counting Kit-8 reagent for 7days (Dojindo Molecular Technologies, Inc., Kumamoto, Japan). Fluorescence images were obtained using a Biozero 800 system (Keyence, Osaka, Japan).

To evaluate encapsulated cell viability, MC3T3-E1 cells at a density of 3×10^6/mL of PLL (0.65) (10% w/v) were cryopreserved by placing the vials in a -80°C freezer for 1 week, and after thawing, the cells in COOH-PLL were mixed with laponite (8% w/v) to form the nanocomposite $N_6P(65)_{1.5}$. Osmolality of the nanocomposite was controlled to physiological conditions (280 mOsm). This nanocomposite was spread as a thin film on a glass-bottom dish (Matsunami Glass IND., LTD., Osaka, Japan), and after 24 h and 72 h of culture, cell viability was determined using a live-dead assay kit (Life Technologies Corp., NY, USA). To further confirm the cell survival activity, after 24 h of encapsulation culture, the nanocomposite including cells was broken down and placed on the TCP, and cell adhesion was observed for 24 h by live-dead assay.

2.9 Statistical analysis

All data are expressed as the mean ± standard deviation (SD). All experiments were conducted in triplicate. A one-way ANOVA with post-hoc Fisher's protected least significant difference test was used for comparison among groups. Differences were considered statistically significant at a $P<0.05$.

3. Results and discussion

3.1 Preparation of polyampholytes and their cryoprotective properties

ε-PLL is a L-lysine homopolymer biosynthesized by *Streptomyces* species [42] and is used as a food additive because of its antimicrobial activities, which are ascribed to the cationic charge of its side-chain α-amino groups [43]. According to our previous research; cytotoxicity decreases with the introduction of carboxyl groups into PLL. The polymer charge can be tuned by varying the level of succination, thus enabling the control of electrostatic interactions

between the drugs and polymer. In the present study, the succination ratio was calculated by ^{1}H NMR (Figure S1, S2, S3). The zeta potential measurement (Figure 2) suggests that the charge on the polymer can be tuned by varying succination levels and pH. For example, PLL (0.65) was positively charged under acidic pH and it became negatively charged as the pH was increased because of the presence of both carboxyl and amino groups in the polymer.

PLL (0.65) is a potent, non-penetrating CPA with low cytotoxicity. COOH-PLL has been shown to exhibit very high cryopreservation efficiency without the addition of any other CPA, and it has been used for the cryopreservation of various cell lines. Figure 3 shows that PLL (0.65) at various concentrations had excellent post-thaw survival efficiency, higher than 90%. The result was in agreement with our previous report [37].

3.2 Nanocomposite formulation

Formulation of nanocomposites involves the incorporation of laponite XLG. In the present study, PLL (0.5, 0.65, and 0.9) was used because it is a polyampholyte and its polymer chains were expected to be intercalated between the laponite discs via electrostatic interactions. Various nanocomposites were prepared by varying the polymer and laponite concentration (Table 1).

3.3 Characterization of the nanocomposite

3.3.1 ATR-FTIR

In the lyophilized nanocomposite, peaks from both the polymer and laponite particles were observed. In Figure 4, the peaks around 3262 cm^{-1} (peptide proton mode of NH-CO of β sheet structure), 2944 cm^{-1} (CH_2 stretching), 1642 cm^{-1} (carbonyl of amide I), and 1529 cm^{-1} (NH bending of amide II) [44] indicate the presence of the polymer and those around 1640, 980, and 650 cm^{-1} show the presence of laponite particles [12]. This result verifies the presence of both PLL (0.65) and laponite moieties within the gels.

3.3.2 XRD measurement

To evaluate the presence of the polymer and laponite in the nanocomposite, XRD analysis was performed. X-ray diffraction patterns of dried gels are presented in Figure 5. The X-ray reflections predominantly correspond to the COOH-PLL intercalated clay, suggesting the presence of polymer-clay stacks in the system [15]. Intercalation of COOH-PLL chains between the clay platelets was deduced by comparing the d-spacing values from the XRD reflections of the layered pure laponite with d-spacing values from the XRD reflections of the layered nanocomposites. The intercalation peak for all the nanocomposites varied according to the pH and charge on the polymer. The difference in d-spacing (Table 2) between the polymer nanocomposite and pure laponite may be attributed to the presence of COOH-PLL chains between the clay platelets.

From the ATR-FTIR and XRD analysis, it can be concluded that a nanocomposite composed of COOH-PLL and laponite can be formulated. In such nanocomposites, the polymer is intercalated between the laponite discs. Based on these two results, the possible structure of the nanocomposite $N_6P(65)_{1.5}$ at pH 7 that was formulated using PLL (0.65) is shown in Figure 6.

3.4 Dynamic mechanical analysis

Figure 7a illustrates the dynamic mechanical analysis of laponite dispersions without polymer when the pH was varied from basic to neutral to acidic. In this system, the concentration of the laponite was fixed to 6% (w/v %). The results indicate the transition of the system from a strong gel to a very weak gel with pH variation. In salt-free water, laponite particles at a higher concentration are stabilized by repulsive interactions. When the interactions are screened by salt, the particles aggregate because of the formation of electrostatic bonds [22].

Laponite dispersions in pure water are always found at pH 10 [45]. When the pH of the laponite dispersion is varied, the concentration of ions in the system changes [46,47]. Thus interplay of ions and rim charge with different pH values of the laponite dispersion leads to different G′ and G″ values.

Figure 7b depicts the change in mechanical strength of nanocomposite $N_6P(65)_{1.5}$ under various pH conditions. G′ was found to be higher than G″ in the experimental frequency region for all of the hydrogels. The maximum value of G′was observed at pH 7 and the minimum value was observed for the nanocomposite prepared at acidic pH. The difference in the mechanical strength of the nanocomposite under varying pH values can be attributed to the presence of COOH-PLL, as zeta potential measurements suggest that PLL (0.65) is negatively charged at pH 7 (Figure 2). Additionally, it is well-known fact that polymers that are long enough to form inter-particle bridges generate a reversible polymer-clay network that dominates the rheological response of the system [23,48,49]. The PLL (0.65) chain is expected to form bridges between nanosilicate discs, as supported by the XRD data (Figure 4 and Table 2). This cross-linking in the laponite-PLL (0.65) system at pH 7 led to the formation of stronger polymer-clay networks. When the pH of this nanocomposite was increased, laponite and PLL (0.65) both were dominated by a high negative charge as previously indicated in the literature and by the present zeta potential measurements, respectively [17,21]. Under basic conditions it was previously reported that laponite particles are largely dominated by repulsive interactions and that a glassy phase is present. Upon the addition of the non-adsorbing polymer, the laponite glass melts and the formation of the arrested state is delayed [50]. In the present study, at pH 12, PLL (0.65), which is highly negatively charged, acted as a non-adsorbing polymer that led to the lower G′ of the nanocomposite as compared to the value at pH 7. Figure 6b shows that the system progressed from a strong gel to a very weak gel state when the pH was reduced. A likely explanation is

that when the polymer and laponite are both positively charged, the face-rim bonds are no longer stable and the system undergoes irreversible change from a strong gel to mechanically weaker gel.

In the current study, we used two other types of polyampholytes PLL (0.5) and PLL (0.9). Nanocomposites were prepared ($N_6P(50)_{1.5}$ and $N_6P(90)_{1.5}$) using these two polyampholytes, respectively. These nanocomposites showed the same results when subjected to changes in pH as depicted in Figure S4 and S5.

Figure 7c illustrates the influence of the manipulation of PLL (0.65) concentration on the G′ and G″ of the nanocomposite for 6% laponite dispersions at pH 7. The mechanical strength increased with polymer concentration, but when the concentration of the polymer was almost the same as that of the laponite, the system changed from a strong gel to mechanically weaker gel, suggesting that as the amount of the polymer increased, the bridging or intercalation between the laponite discs and the polymer also increased, leading to a higher G′. However, when the polymer concentration was too high, then the rheological behavior of the nanocomposite was representative of a very weak gel, possibly because of increased steric hindrance of the adsorbed polymer that leads to unstable face-rim bonds and transformation to a lower mechanical strength [22].

Figure 7d shows the effect of manipulating the laponite concentration on G′ and G″ when the PLL (0.65) concentration was fixed to 1.5%. The results indicate that the mechanical strength of the nanocomposite can be tuned by varying the laponite concentration. Mechanically stronger gels were obtained at higher laponite concentrations because of the presence of more crosslinking points and relatively weaker gels were obtained at lower laponite concentrations because the crosslinking density was reduced with a decrease in laponite concentration.

Figure 8 shows the tunable mechanical properties of the nanocomposite $N_6P_{1.5}$ at pH 7, formulated using PLL with various degrees of succination. This figure shows that the

mechanical strength of the nanocomposite can be easily tuned from 4 to 10 kPa by varying the succination ratio in the polymer.

Thixotropic hydrogels are viscoelastic materials that behave as liquids when subjected to shear stress and then return to the liquid state when the stress is removed. This property is time-dependent, ranging from many minutes in the case of breakdown to many hours in the case of reconstruction [51]. Therapeutics can be incorporated in these materials ex vivo, and then they can be injected in vivo by shear-induced flow [13]. In our current study, we formulated nanocomposites that were loaded with cells. Structural changes and recovery in these hydrogels were estimated using a hysteresis loop [52]. In these experiments, the shear rate was first increased to the maximum, value followed by a decrease to the initial start value. The area within the two curves is defined as the hysteresis loop and indicates the potential speed of the sol-gel transition. A larger area reflects a longer recovery time. The graph of the nanocomposite composed of $N_6P(65)_{1.5}$ at pH 7 shows structural recovery and suggests that the nanocomposite of this study can be return to its original shape after one hour (Figure 9) and thus can be used for various biomedical purposes. Figure 10 (a) shows the behavior of the polymer-clay nanocomposite that we believe occurred during the hysteresis loop experiment. When the nanocomposite was loaded onto the rheometer plate before application of shear, the entire system was at rest. It is expected that the system consisted of a network between randomly oriented laponite discs and polyampholyte chains that acted as cross-links between laponite discs. When shear was applied, polymer chains were desorbed from the rim and adopted various conformations such as trains and loops, thus imparting flow to the system and converting it from gel to sol. When the shear was removed, the system tried to regain its original structure.[15] These materials can be injected through 20-25 gauge needles as shown in Figure 10 (b).

3.5 Cell adhesion and viability

In addition to tunable physical and chemical properties, cell adhesion is important for biomedical applications. Synthetic hydrogels are hydrophilic and are usually inert towards protein or cell adhesion. Adhesion was previously achieved by tethering of short oligopeptides, such as RGD or whole proteins, to the polymer [53]. However, introduction of laponite to the polymer is a simple and efficient approach for achieving cell adhesion [54,55]. Here, MC3T3-E1 cells were seeded onto the nanocomposites and the cell adhesion was evaluated 7 days after seeding. Nanocomposites with lower laponite concentrations (2% or 1%) were too weak to handle. Therefore, we fabricated nanocomposites with a minimum laponite concentration of 3%. Figure 11 (a) and 11 (b) show that cell adhesion can be controlled by varying the laponite concentration to 3 and 6 %, respectively. The current injectable hydrogels not only support cell adhesion in a manner similar to that of TCP (Figure 11 (c)) but also promote facile proliferation of cells, as shown in Figure 11 (d), which could enable them to be used as an injectable cell carrier. Nanocomposites with a higher laponite concentration show better cell proliferation than those with a lower laponite concentration. In the current study, laponite was used as a cross-linker for the polyampholyte laden with cells. Introduction of laponite converts the system from a liquid to gel. Therefore, the cell adhesion property of this nanocomposite can be attributed to laponite. These silicates are complex poly-ions that contain magnesium, which promotes cell adhesion, differentiation, spreading, and migration [56].

Cryopreserved MC3T3-E1 cells in 10% PLL (0.65) were easily encapsulated by simply mixing the PLL (0.65) after thawing with laponite. Cell viability was evaluated after certain time intervals. Figure 12 (a) shows no cell death in the nanocomposites. The nanocomposites were cytocompatible and the cells remained viable when cultured in the nanocomposite for 72 h Figure 12 (b). Cells were viable in the nanocomposite even after 15-20 days (data not

shown). Because cell density was relatively low in the experiments shown in Figure 12 (a) and (b) because of dilution after cryopreservation, we further confirmed the cell adhesion on TCP after encapsulation culture. Figure 12 (c) shows that the cells seeded after encapsulation culture in the nanocomposite for 24 h were alive and spread at 24 h, and the red spots indicate hydrogel fragments stained with ethidium homodimer. The improved cell adhesion and cell viability in the nanocomposites demonstrates that this system can potentially be applied for cell delivery directly after cryopreservation.

Cell harvesting and cell maintenance are serious barriers to tissue engineering for cell delivery applications and need to be addressed. To produce off-the-shelf tissue-engineered constructs, cryopreservation is necessary. Washing out CPA immediately after thawing causes unnecessary cell loss, and subsequent encapsulation of cells in hydrogels is still in its infancy and requires optimization. In this study, we formulated a thixotropic and injectable nanocomposite using a polyampholyte CPA and laponite. No previous study has emphasized the cryopreservation of cells until immediately before usage, where after thawing, they can be injected into the defect site without the need to wash out the CPA. Given the thixotropic nature of the nanocomposite, it can easily be injected even after gel formation, which helps prevent the loss of the biomaterial to undesired areas. In this study, mouse preosteoblast cells were cryopreserved with COOH-PLL, and after thawing, the CPA-laden cells were mixed with laponite in appropriate amounts to form smart hydrogels in which the cells remained viable; the hydrogels also showed thixotropicity, biocytocompatibility, and tunable mechanical properties. Overall, our current findings suggest that this system can be employed for cell delivery applications.

4. Conclusions

In this study, we constructed a novel system that has a range of potential biomedical and biotechnological applications. To our knowledge, this is the first study on the interaction between polyampholytes and laponite. This is a fundamental study that unveils the interaction of the polyampholyte with laponite under various conditions, which can be useful for the formulation of new scaffolds in the future. The interplay of the charges on the two components of the nanocomposite enables good control over the mechanical properties. The system's switching ability from strong gel to very weak gel with a change in pH opens new avenues for cell delivery applications. This study overcomes the first developmental challenge for smart hydrogels by mixing cells immediately after thawing with laponite, which results in a nanocomposite that can easily be injected by applying pressure. This system does not require any pretreatment of cells before injection, making cell maintenance after thawing unnecessary. However, the nanocomposite did not have a high storage modulus and is thus applicable for soft materials only. In the pursuit of an injectable, thixotropic cell scaffold with modifiable mechanical properties, we have engineered a simple and effective nanocomposite that can be tailored to specific functionalities for various tissue-engineering applications.

Supplementary figures

Supplementary data for this article can be found online.

Acknowledgements

This study was supported in part by a Grant-in-Aid, KAKENHI (25242050), for Scientific Research from the Ministry of Education, Culture, Sports, Science and Technology, Japan

References

[1] J. K. Carrow, A. K. Gaharwar, Bioinspired polymeric nanocomposites for regenerative medicine, Macromol. Chem. Phys. 216 (2015) 248-264.

[2] A. K. Gaharwar, N. A. Peppas, A. Khademhosseini, Nanocomposite hydrogels for biomedical applications, Biotechnol. Bioeng. 111 (2014) 441-453.

[3] R. C. Thompson, M. J. Yaszemski, J. M. Powers, A.G. Mikos, Hydroxyapatite fiber reinforced poly(-hydroxy ester) foams for bone regeneration, Biomaterials. 19 (1998) 1935-1943.

[4] R. Zhang, P. X. Ma, Poly(a-hydroxyl acids)/hydroxyapatite porous composites for bone tissue engineering. I. Preparation and morphology, J. Biomed. Mater. Res. 44 (1999) 446-455.

[5] H. H. Lu, S. F. El-Amin, K. D. Scott, C. T. Laurencin, Three-dimensional, bioactive, biodegradable, polymer-bioactive glass composite scaffolds with improved mechanical

properties support collagen synthesis and mineralization of human osteoblast-like cells in vitro, J. Biomed. Mater. Res. 64A (2003) 465-474.

[6] S. S. Kim, K. M. Ahn, M. S. Park, J. H. Lee, C. Y. Choi, B. S. Kim, A poly(lactide coglycolide)/hydroxyapatite composite scaffold with enhanced osteoconductivity, J. Biomed. Mater. Res. 80A (2007) 206-215.

[7] L. L. Hench, R. J. Splinter, W. C. Allen, T. K. Greenlee, Bonding mechanisms at the interface of ceramic prosthetic materials, J. Biomed. Mater. Res. 5 (1971) 117-141.

[8] L. L. Hench, Bioceramics. J. Am. Ceram. Soc. 81 (1998) 1705-1728.

[9] W. Huang, D. E. Day, K. Kittiratanapiboon, M. N. Rahaman, Kinetics and mechanisms of the conversion of silicate (45S5), borate, and borosilicate glasses to hydroxyapatite in dilute phosphate solution, J. Mater. Sci. Mater. Med. 17 (2006) 583-596.

[10] A. Khademhosseini, R. Langer, J. Borenstein, J. Vacanti, Microscale technologies for tissue engineering and biology, Proc. Natl. Acad. Sci. U.S.A. 103 (2006), 2480-2487.

[11] A. K. Gaharwar, C. P. Rivera, C. J. Wu, G. Schmidt, Transparent, elastomeric and tough hydrogels from poly(ethylene glycol) and silicate nanoparticles, Acta Biomater. 7 (2011) 4139-4148.

[12] C. W. Chang, A. Spreeuwel, C. Zhang, S. Varghese, PEG/clay nanocomposite hydrogel: a mechanically robust tissue engineering scaffold, Soft Matter. 6 (2010) 5157- 5164.

[13] H. D. Lu, D. E. Soranno, C. B. Rodell, I. L. Kim, J. A. Burdick, Secondary Photocrosslinking of Injectable Shear-Thinning Dock-and-Lock Hydrogels, Adv. Healthcare Mater. 2 (2013) 1028-1036.

[14] A. K. Gaharwar, V. Kishore, C. Rivera, W. Bullock, C. J. Wu, O. Akkus, G. Schmidt, Physically Crosslinked Nanocomposites from Silicate-Crosslinked PEO: Mechanical Properties and Osteogenic Differentiation of Human Mesenchymal Stem Cells, Macromol. Biosci. 12 (2012) 779-793.

[15] E. A. Stefanescu, C. Stefanescu, W. H. Daly, G. Schmidt, L. L. Negulescu, Hybrid polymer–clay nanocomposites: a mechanical study on gels and multilayered films, Polymer. 49 (2008) 3785-3794.

[16] K. Haraguchi, H. J. Li, K. Matsuda, T. Takehisa, E. Elliott, Mechanism of Forming Organic/Inorganic Network Structures during In-situ Free-Radical Polymerization in PNIPA-Clay Nanocomposite Hydrogels, Macromolecules. 38 (2005) 3482-3490.

[17] B. Jonsson, C. Labbez, B. Cabane, Interaction of nanometric clay platelets, Langmuir. 24 (2008) 11406-11413.

[18] M. Kroon, W. L. Vos, G. H. Wegdam, Structure and formation of a gel of colloidal disks, Phys. Rev. E. 57 (1998) 1962-1970.

[19] M. Morvan, D. Espinat and J. Lambard, Th. Zemb, Ultrasmall- and small-angle X-ray scattering of smectite clay suspensions, Colloids Surf. A. 82 (1994) 193-203.

[20] Laporte Industries Ltd., Laponite Technical Bulletin. 1990, L104/90/A, p. 1

[21] S. L. Tawari, D. L. Koch, C. Cohen, Electrical Double-Layer Effects on the Brownian Diffusivity and Aggregation Rate of Laponite Clay Particles, J. Colloid Interface Sci. 240 (2001) 54-66.

[22] C. Martin, F. Pignon, J. M. Piau, A. Magnin, P. Lindner, B. Cabane, Dissociation of thixotropic clay gels, Phys. Rev. E. 66 (2002) 021401.

[23] P. Mongondry, T. Nicolai, J. F. Tassin, Influence of pyrophosphate or polyethylene oxide on the aggregation and gelation of aqueous laponite dispersions, J. Colloid Interface Sci. 275 (2004) 191-196.

[24] J. Labanda, J. Sabat´e, J. Llorens, Rheology changes of Laponite aqueous dispersions due to the addition of sodium polyacrylates of different molecular weights, Colloids Surf. A. 301 (2007) 8-15.

[25] M. Shen, L. Li, Y. Sun, J. Xu, X. Guo, R. K. Prud'homme, Rheology and Adhesion of Poly(acrylic acid)/Laponite Nanocomposite Hydrogels as Biocompatible Adhesives, Langmuir. 30 (2014) 1636-1642.

[26] J. R. Xavier, T. Thakur, P. Desai, M. K. Jaiswal, N. Sears, E. C. Hernandez, R. Kaunas, A. K. Gaharwar, Bioactive Nanoengineered Hydrogels for Bone Tissue Engineering: A Growth-Factor-Free Approach, ACS Nano. 9 (2015) 3109-3118.

[27] S. E. Kudaibergenov, Recent advances in the study of synthetic polyampholytes in solutions, Advances in Polym. Sci. 144 (1999) 115-197.

[28] E. A. Bekturov, S. E. Kudaibergenov, S. R. Rafikov, Synthetic polymeric ampholytes in solution, J. Macromol. Sci., Part C: Polym. Rev. 30 (1990) 233.

[29] Z. Tao, C. Kaimin, G. Hongchen, Investigations on the Interactions of Proteins with Polyampholyte-Coated Magnetite Nanoparticles, J. Phys. Chem. B. 2013, 117, 14129.

[30] R. Rajan, M. Jain, K. Matsumura, Cryoprotective properties of completely synthetic polyampholytes via reversible addition-fragmentation chain transfer (RAFT) polymerization and the effects of hydrophobicity, J. Biomater. Sci. Polym. Ed. 24 (2013) 1767-1780.

[31] K. Matsumura, K. Kawamoto, M. Takeuchi, S. Yoshimura, D. Tanaka, S. H. Hyon, Cryopreservation of a Two-Dimensional Monolayer Using a Slow Vitrification Method with Polyampholyte to Inhibit Ice Crystal Formation, ACS Biomater. Sci. Eng. 2 (2016) 1023–1029.

[32] M. Maehara, M. Sato, M. Watanabe, H. Matsunari, M. Kokubo, T. Kanai, M. Sato, K. Matsumura, S. H. Hyon, M. Yokoyama, J. Mochida, H. Nagashima, Development of a novel vitrification method for chondrocyte sheets, BMC Biotechnology. 13 (2013) 58.

[33] K. Matsumura, F. Hayashi, T. Nagashima, S. H. Hyon, Long-term cryopreservation of human mesenchymal stem cells using carboxylated poly-L-lysine without the addition of proteins or dimethyl sulfoxide, J. Biomater. Sci. Polym. Ed. 24 (2013)1484-1497.

[34] K. Matsumura, J. Y. Bae, S. H. Hyon, Polyampholytes as cryoprotective agents for mammalian cell cryopreservation, Cell Transplant. 19 (2010) 691-699.

[35] R. Rajan, F. Hayashi, T. Nagashima, K. Matsumura, Toward a Molecular Understanding of the Mechanism of Cryopreservation by Polyampholytes: Cell Membrane Interactions and Hydrophobicity, Biomacromolecules. 17 (2016) 1882-1893.

[36] R. Rajan, K. Matsumura, A zwitterionic polymer as a novel inhibitor of protein aggregation, J. Mater. Chem. B. 3 (2015) 5683-5689.

[37] K. Matsumura, S. H. Hyon, Polyampholytes as low toxic efficient cryoprotective agents with antifreeze protein properties, Biomaterials. 30 (2009) 4842-4849.

[38] M. Jain, R. Rajan, S. H. Hyon, K. Matsumura, Hydrogelation of dextran-based polyampholytes with cryoprotective properties via click chemistry, Biomater. Sci. 2 (2014) 308-317.

[39] A. F. Haneeb, Determination of free amino groups in proteins by trinitrobenzenesulfonic acid, Anal. Biochem. 14 (1966) 328-336.

[40] P. Ehrlich, Address in Pathology, ON CHEMIOTHERAPY, Br. Med. J. 5 (1913) 353-359.

[41] C. R. Prull, Part of a Scientific Master Plan?Paul Ehrlich and the Origins of his Receptor Concept, Med. Hist. 47 (2003) 332-356.

[42] Y. Yamanaka, C. Maruyama, H. Takagi, Y. Hamano, Epsilon-poly-L-lysine dispersity is controlled by a highly unusual nonribosomal peptide synthetase, Nat. Chem. Biol. 4 (2008) 766-772.

[43] M. Saimura, M. Takehara, S. Mizukami, K. Kataoka, H. Hirohara, Biosynthesis of nearly monodispersed poly(epsilon-L-lysine) in Streptomyces species, Biotechnol. Lett. 30 (2008) 377-385.

[44] M. Rozenberg, G. Shoham, FTIR spectra of solid poly-l-lysine in the stretching NH mode range, Biophys. Chem. 2007, 125, 166.

[45] H. Z. Cummins, Liquid, glass, gel: the phases of colloidal laponite, J. Non-Cryst. Solids. 353 (2007) 3891-3905.

[46] T. Nicolai, S. Cocard, Structure of gels and aggregates of disk-like colloids, Eur. Phys. J. E. 5 (2001) 221-227.

[47] T. Nicolai, S. Cocard, Dynamic Light-Scattering Study of Aggregating and Gelling Colloidal Disks, J. Colloid Interf. Sci. 244 (2001) 51-57.

[48] J. Lal, L. Auvray, Interaction of polymer with clays, J. Appl. Crys. 33 (2000) 673-676.

[49] J. Lal, L. Auvray, Interaction of polymer with discotic clay particles, Mol. Cryst. Liq. Cryst. 356 (2001) 503-515.

[50] T. Eckert, R. Bratsch, Re–entrant glass transition in a colloid polymer mixture with depletion attraction, Phys. Rev. Lett. 89 (2002) 125701.

[51] H. A. Barnes, Thixotropy-a review, J. Non-Newtonian Fluid Mech. 70 (1997) 1-33.

[52] R. F. Ker, The time-dependent mechanical properties of the human heel pad in the context of locomotion, J. Exp. Biol. 199 (1996) 1501-1508.

[53] M. Obara, M. S. Kang, K. M. Yamada, Site-directed mutagenesis of the cell-binding domain of fibroneetion: separable, synergistic sites mediate adhesive function, Cell. 53 (1998) 649-657.

[54] P. Schexnailder, A. K. Gaharwar, R. Bartlett, B. L. Seal, G. Schmidt, Tuning Cell Adhesion by Incorporation of Charged Silicate Nanoparticles as Cross-Linkers to Polyethylene Oxide, Macromol. Biosci. 10 (2010) 1416-1423.

[55] M. Jain, K. Matsumura, Polyampholyte- and nanosilicate-based soft bionanocomposites with tailorable mechanical and cell adhesion properties, J. Biomed. Mater. Res. A. 104 (2016) 1379-1386.

[56] S. M. Mihaila, A. K. Gaharwar, R. L. Reis, A. Khademhosseini, A. P. Marques, M. E. Gomes, Silicate Nanoplatelets Enhance the Osteogenic Differentiation of SSEA-4 Positive Selection of Human Adipose Derived Stem Cells, Biomaterials. 35 (2014) 9087-9099.

Table 1. Various nanocomposites prepared by varying the polymer and laponite concentrations.

N_X (w/v)%	**P_z (w/v)%, P: PLL (0.65)**
3	1.5
5	1.5
6	1.5
6	2
6	3
6	5
6	6
6	1.5*
6	1.5**

** PLL (0.5), ** PLL (0.9)*

Table 2. d-spacing of nanocomposites of different polyampholytes with 6% laponite at various pH values.

	pH	**d (nm)**

(Laponite) N_6P_o	7	1.3
$N_6P\ (65)_{1.5}$	7	1.7
	12	1.6
$N_6P\ (50)_{1.5}$	7	1.5
	12	1.7
$N_6P\ (90)_{1.5}$	7	1.9
	12	1.7

Figure Captions

Scheme 1. Schematic representation of PLL succination.

Figure 1. Schematic representation of thixotropic nanocomposite formation.

Figure 2. Zeta potential measurement of different polyampholytes at different pH values.

Figure 3. Cryoprotective property of PLL (0.65). The viability of MC3T3-E1 cells cryopreserved at various concentrations of PLL (0.65) was measured immediately after thawing. The osmotic pressure was adjusted with 10% (w/w) NaCl aqueous solution. NS: not significant.

Figure 4. ATR-FTIR spectra of laponite, pH 7 (top); lyophilized nanocomposite $N_6P(65)_{1.5}$, pH 7 (middle); and PLL (0.65), pH 7 (bottom).

Figure 5. XRD patterns of nanocomposites of different polyampholytes with 6% laponite at various pH values.

Figure 6. Illustration of nanocomposite formed by laponite and PLL (0.65).

Figure 7. Storage and loss moduli of nanocomposites under various conditions at 37˚C: (a) laponite with pH manipulation and without the polymer. (b) $N_6P(65)_{1.5}$ with pH manipulation; P: PLL (0.65). (c) PLL (0.65) with concentration manipulation, pH 7. (d)

laponite concentration manipulation with polymer; P: PLL (0.65), pH 7. Symbols represent the average for n= 3.

Figure 8. Comparison of storage and loss moduli of nanocomposites at pH 7, 37˚C, comprising PLL with different extents of succination.

Figure 9. Thixotropic properties of the nanocomposite $N_6P(65)_{1.5}$ were evaluated using the hysteresis loop test at 37˚C. The figure shows the structural recovery of the nanocomposite.

Figure 10. (a) Schematic representation of the fate of the $N_6P(65)_{1.5}$ nanocomposite in the hysteresis loop test. (b) Illustration of the nanocomposite $N_6P(65)_{1.5}$ that can be injected through a 22G needle.

Figure 11 MC3T3-E1 cell proliferation on nanocomposite hydrogels. Fluorescent microphotographs of phalloidin binding to F-actin of cells cultured on a) $N_3P(65)_{1.5}$, b) $N_6P(65)_{1.5}$, c) tissue culture plate as a control for 7 days, and d) growth curves on these hydrogels. Scale bars represent 100 μm.

Figure 12. Cell viability of MC3T3-E1 cells after a) 24 and b) 72 hours in the nanocomposite $N_6P(65)_{1.5}$. Almost all cells were alive. c) Cells at 24 hours after seeding for encapsulation in the nanocomposite hydrogel. Scale bars represent 100 μm. Almost all cells were alive. Scale bars represent 100 μm.

Graphical abstract

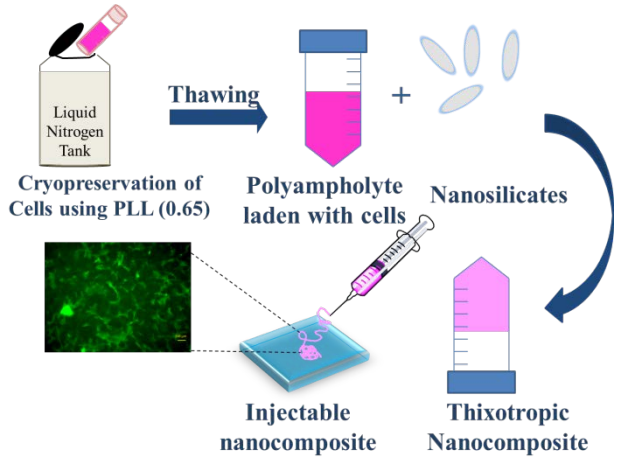

A novel thixotropic, cytocompatible and injectable nanocomposite hydrogel with tunable mechanical properties directly after cryopreservation was formulated using an efficient polymer cryoprotectant and laponite. This is an efficient system in which cells remain viable and can proliferate even after one week. The combined use of thixotropy and cytocompatibility enables this system to be used for cell delivery applications.

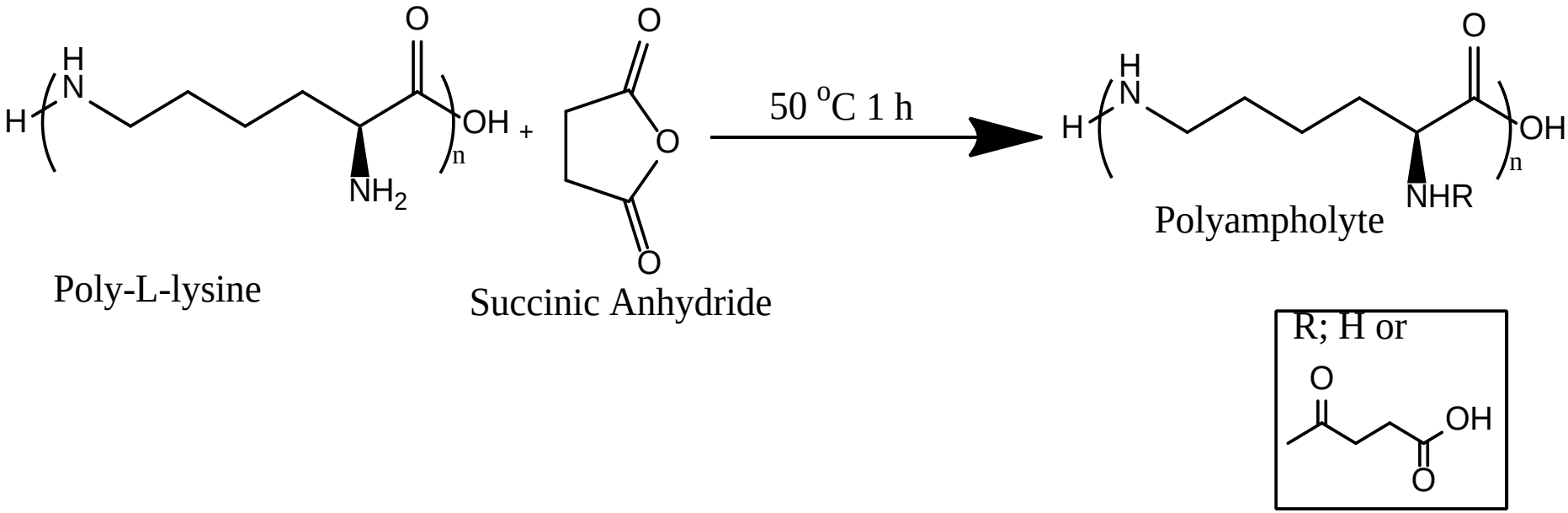

Scheme 1. Schematic representation of PLL succination.

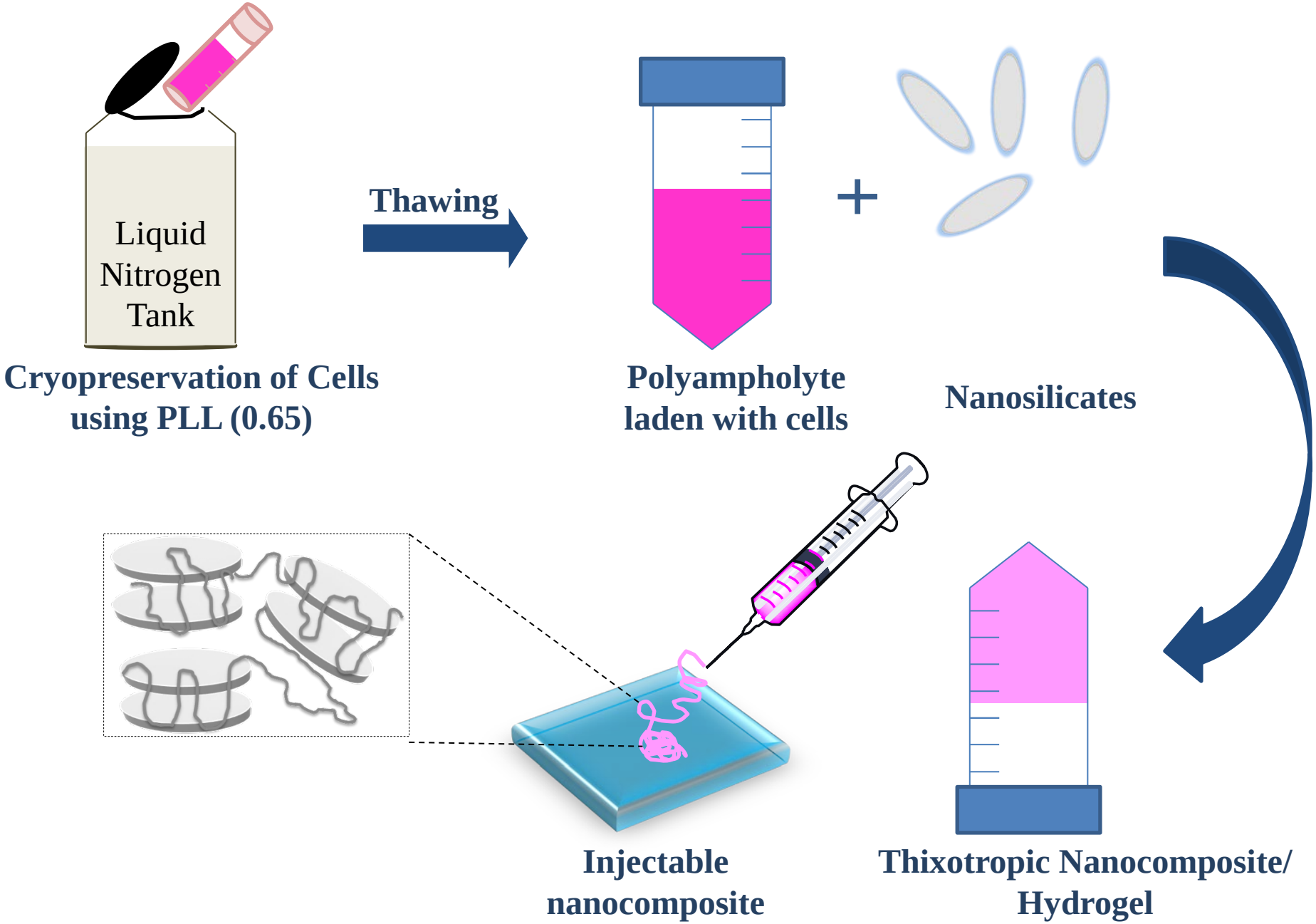

Figure 1. Schematic representation of thixotropic nanocomposite formation.

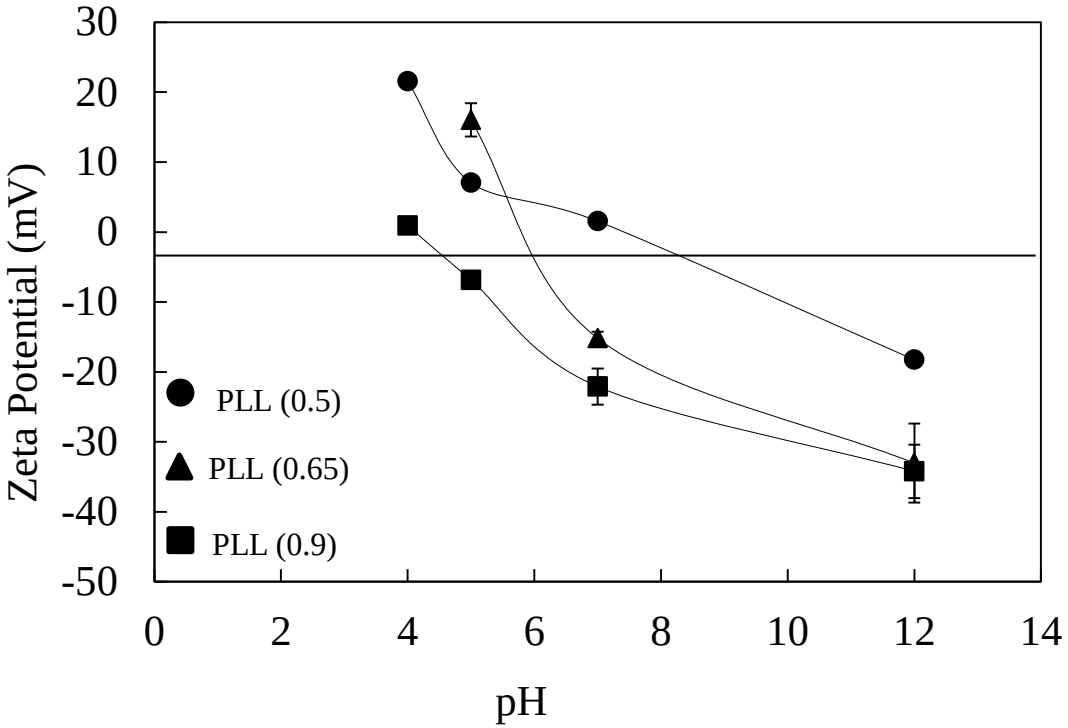

Figure 2. Zeta potential measurement of different polyampholytes at different pH values.

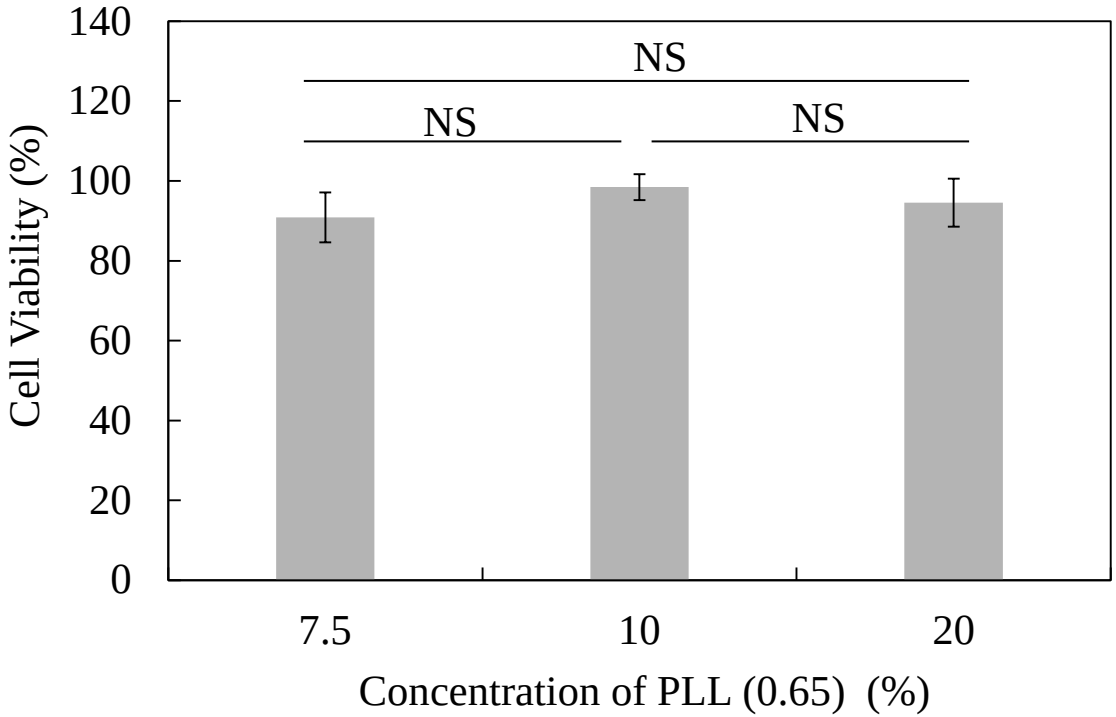

Figure 3. Cryoprotective property of PLL (0.65). The viability of MC3T3-E1 cells cryopreserved at various concentrations of PLL (0.65) was measured immediately after thawing. The osmotic pressure was adjusted with 10% (w/w) NaCl aqueous solution. NS: not significant.

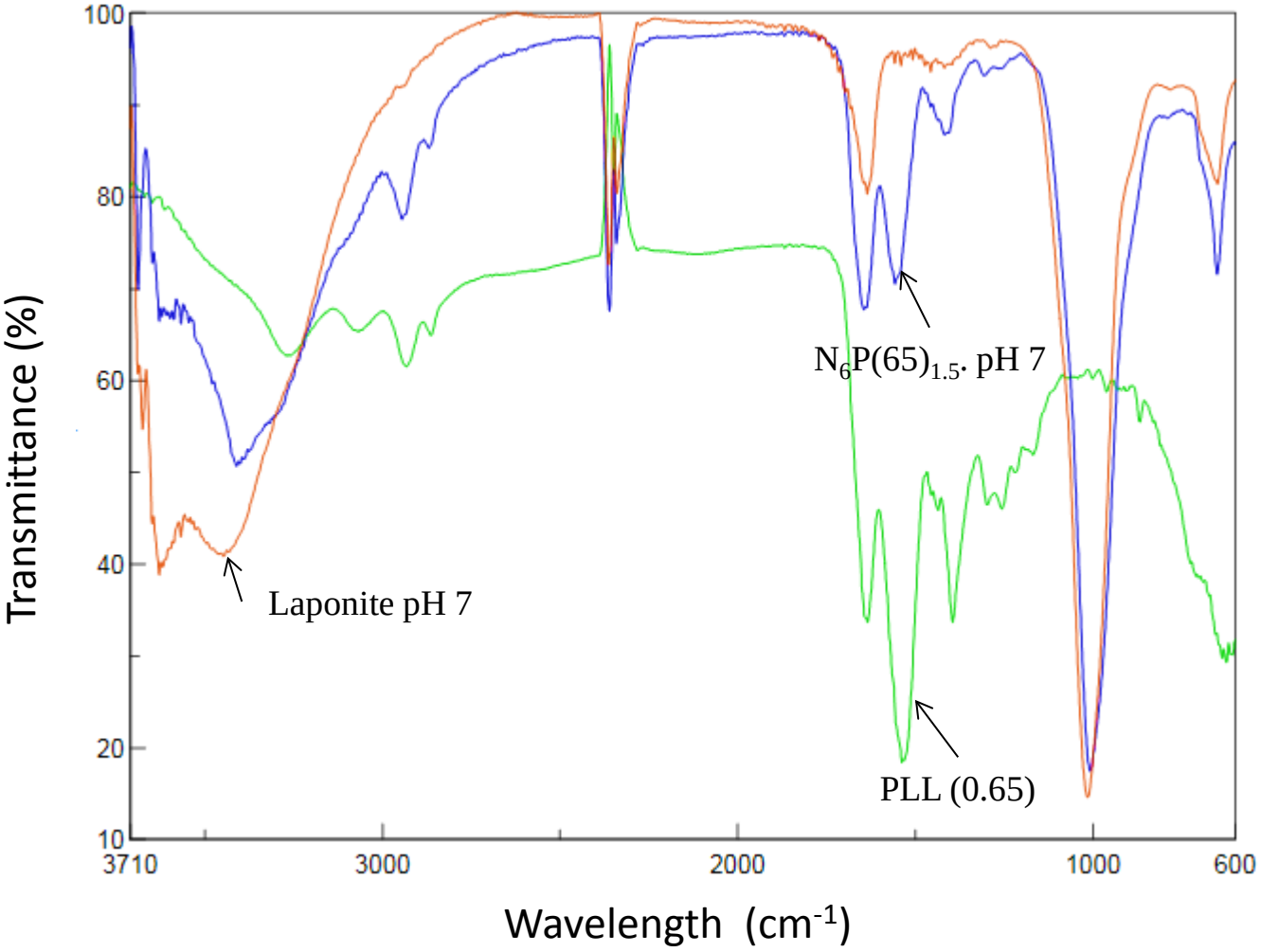

Figure 4. ATR-FTIR spectra of laponite, pH 7 (top); lyophilized nanocomposite $N_6P(65)_{1.5}$, pH 7 (middle); and PLL (0.65), pH 7 (bottom).

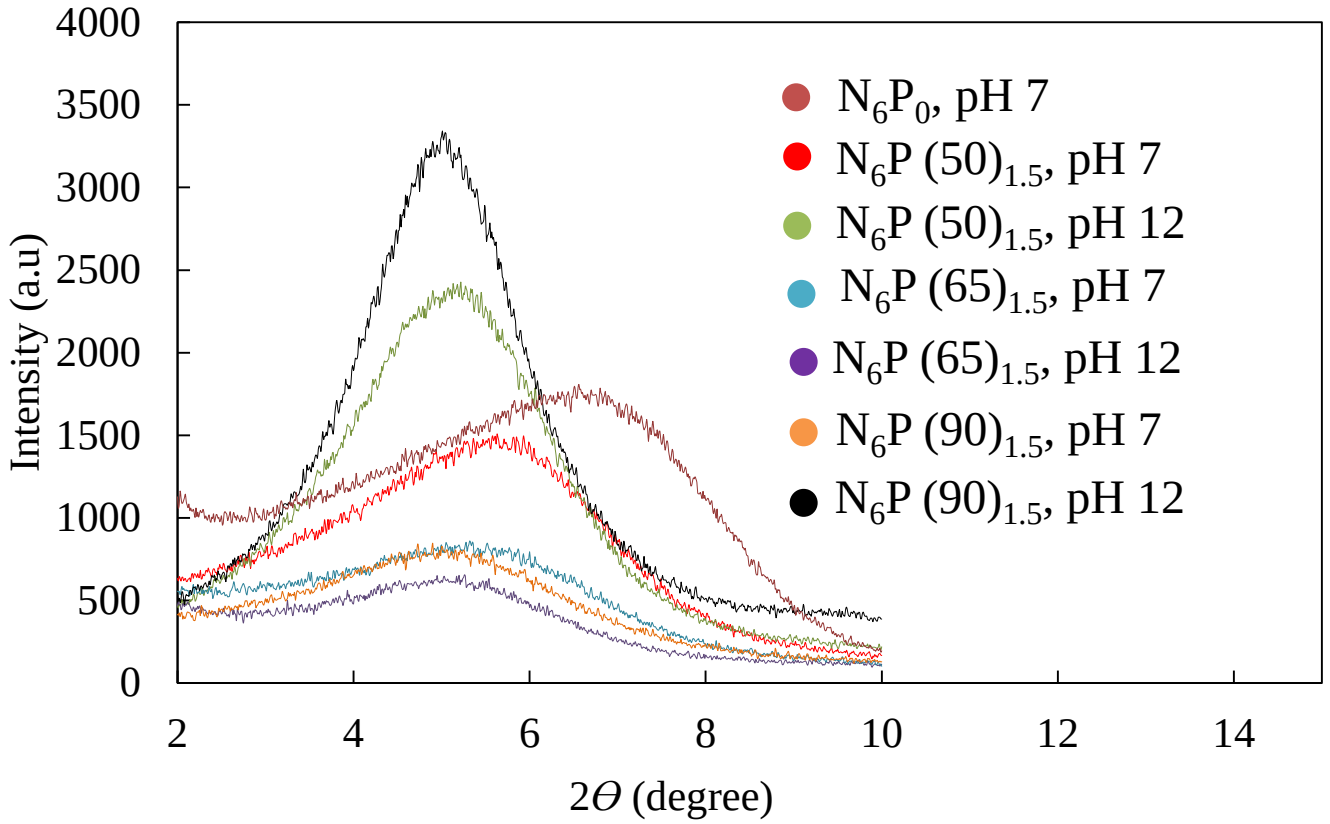

Figure 5. XRD patterns of nanocomposites of different polyampholytes with 6% laponite at various pH values.

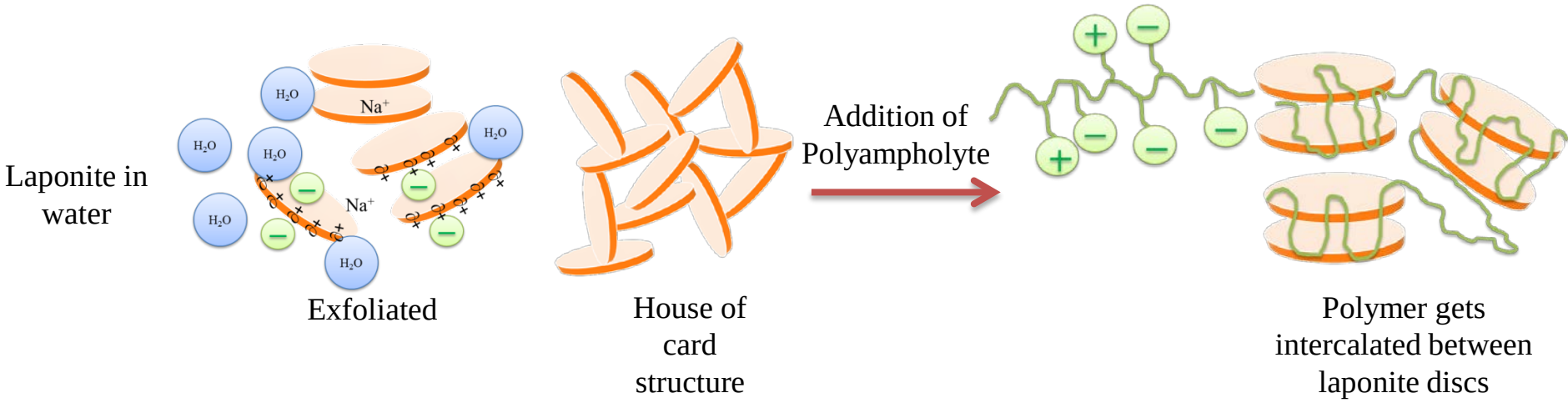

Figure 6. Illustration of nanocomposite formed by laponite and PLL (0.65).

a) 6wt% laponite

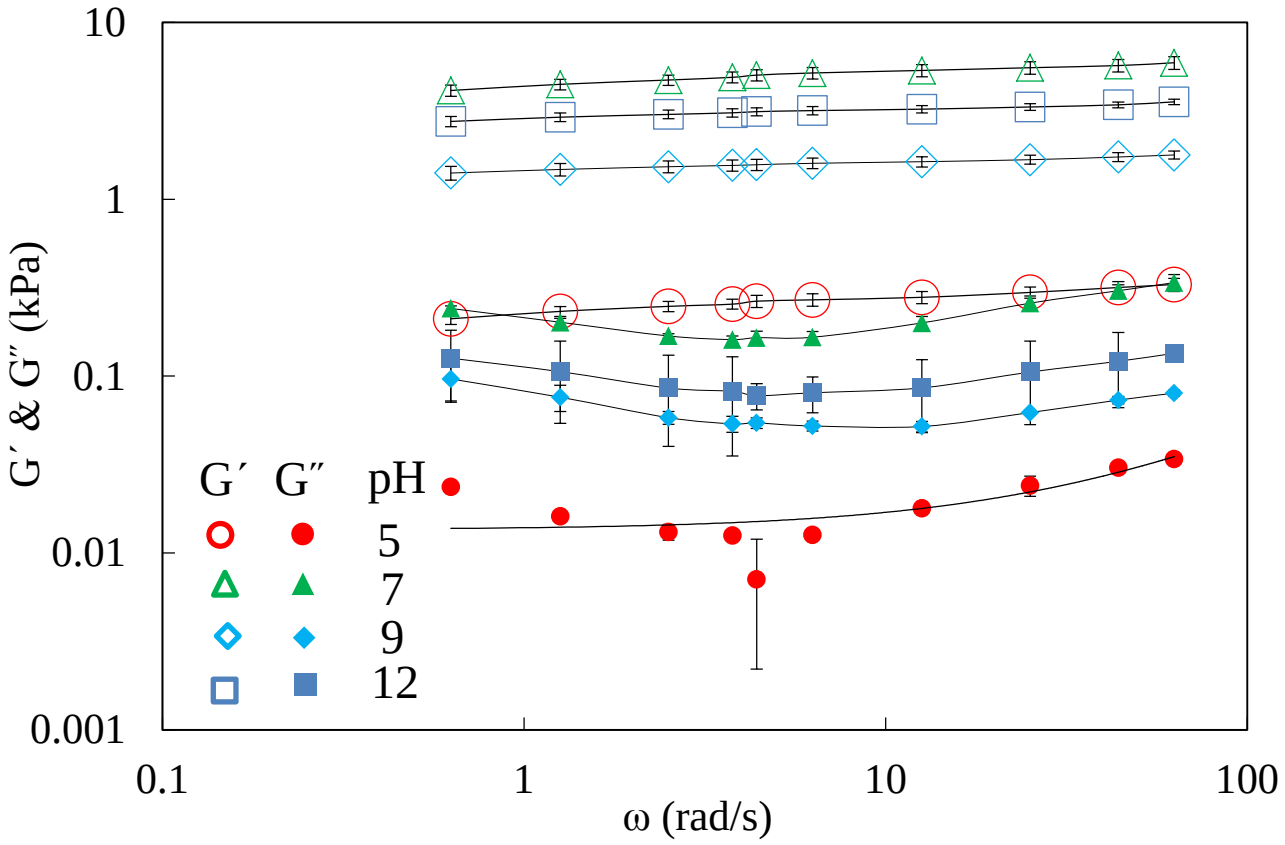

b) $N_6P(65)_{1.5}$

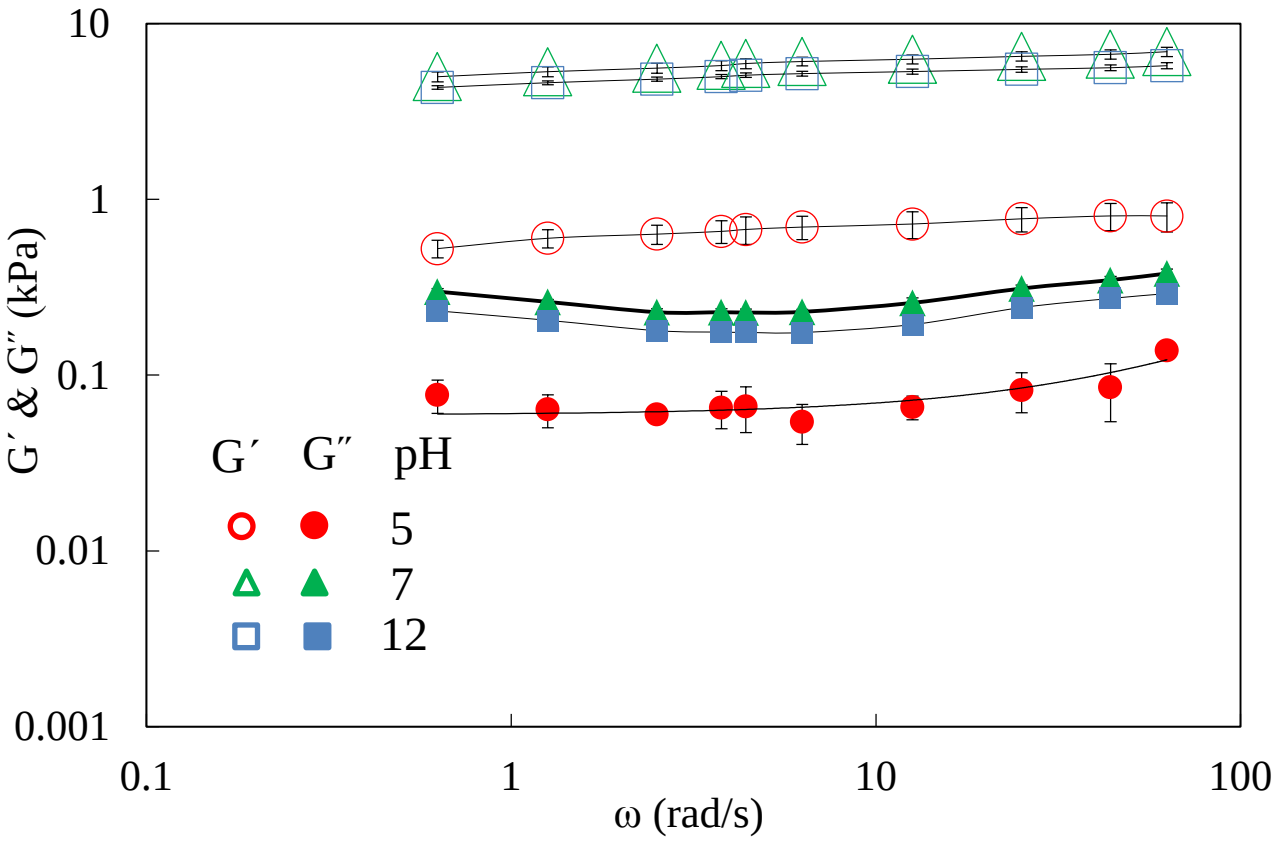

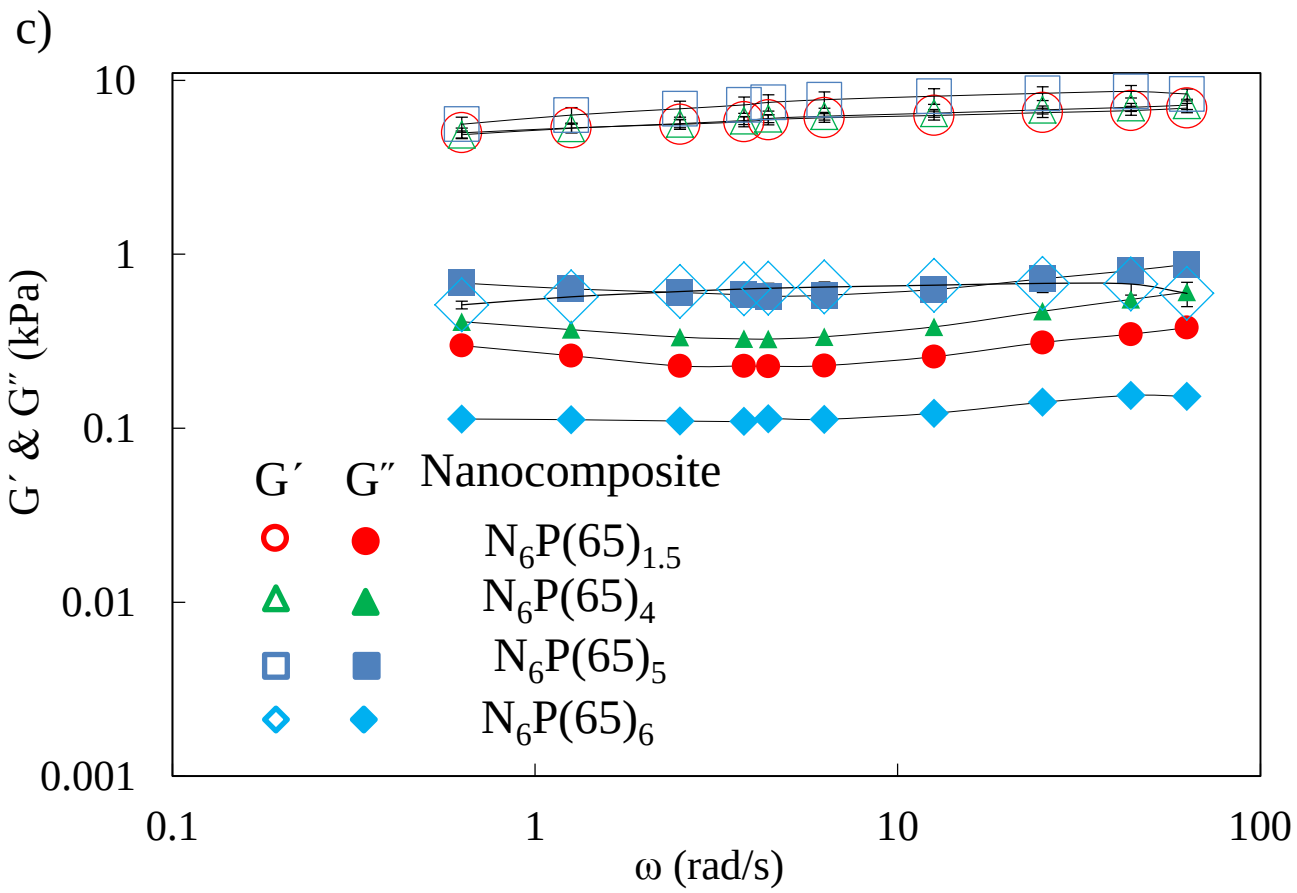
c)
10
1
0.1
0.01
0.001
G′ & G″ (kPa)
0.1
1
10
100
ω (rad/s)
G′
G″
Nanocomposite
N6P(65)1.5
N6P(65)4
N6P(65)5
N6P(65)6

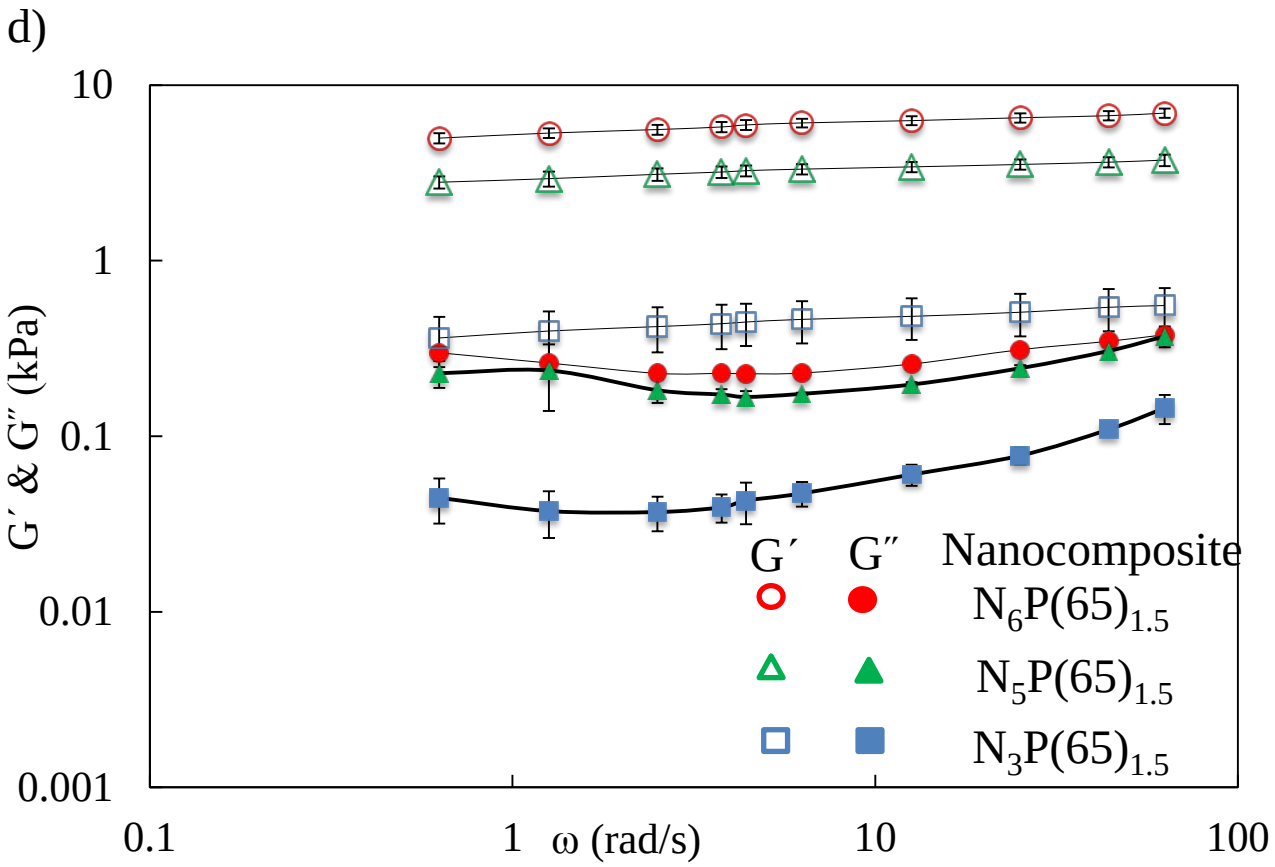

Figure 7. Storage and loss moduli of nanocomposites under various conditions at 37˚C: (a) laponite with pH manipulation and without the polymer. (b) $N_6P(65)_{1.5}$ with pH manipulation; P: PLL (0.65). (c) PLL (0.65) with concentration manipulation, pH 7. (d) laponite concentration manipulation with polymer; P: PLL (0.65), pH 7. Symbols represent the average for n= 3.

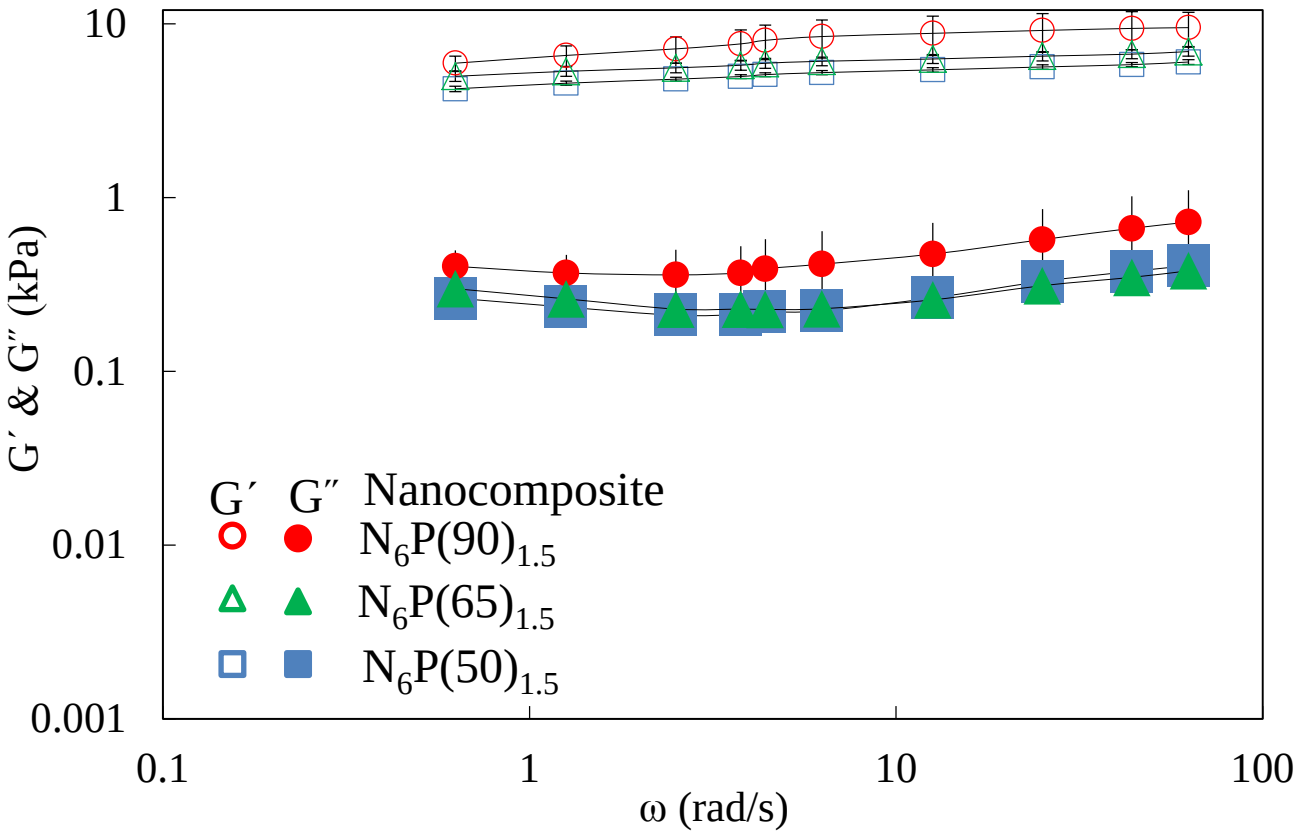

Figure 8. Comparison of storage and loss moduli of nanocomposites at pH 7, 37˚C, comprising PLL with different extents of succination.

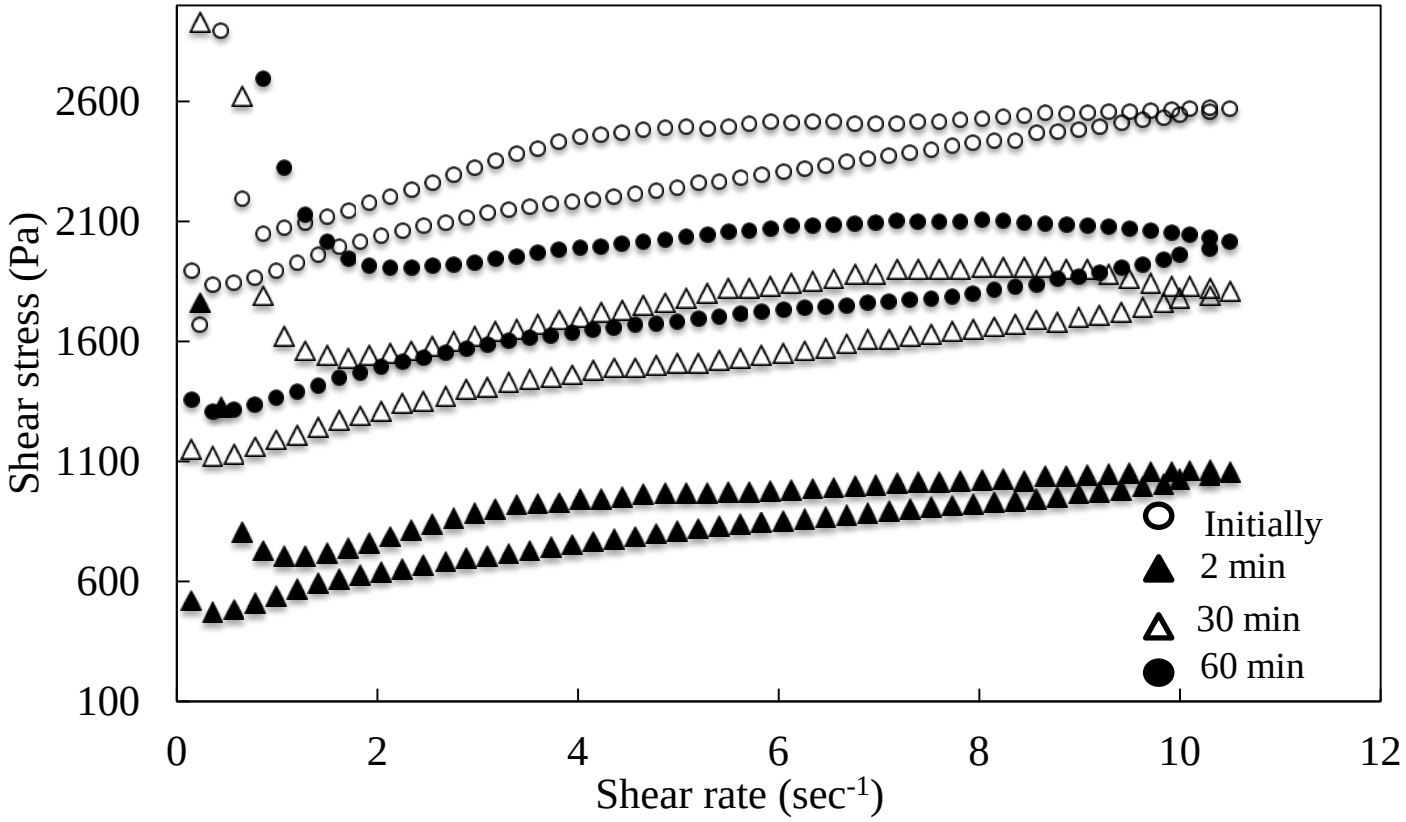

Figure 9. Thixotropic properties of the nanocomposite $N_6P(65)_{1.5}$ were evaluated using the hysteresis loop test at 37˚C. The figure shows the structural recovery of the nanocomposite.

a)

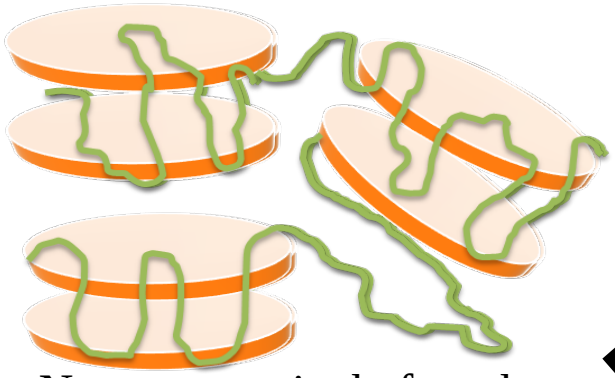

Nanocomposite before the application of shear-stress

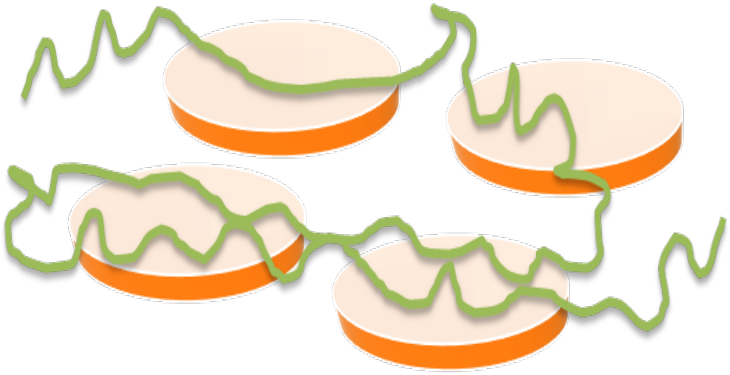

Nanocomposite during the application of shear-stress

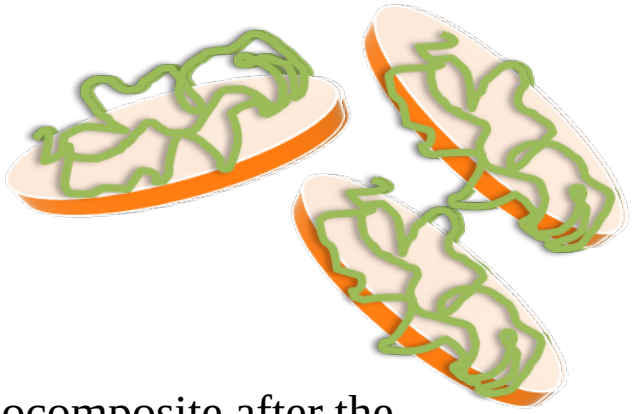

Nanocomposite after the application of shear-stress

Polymer after certain period of time regains its original conformation; leads to structural recovery

b)

Figure 10. (a) Schematic representation of the fate of the $N_6P(65)_{1.5}$ nanocomposite in the hysteresis loop test. (b) Illustration of the nanocomposite $N_6P(65)_{1.5}$ that can be injected through a 22G needle.

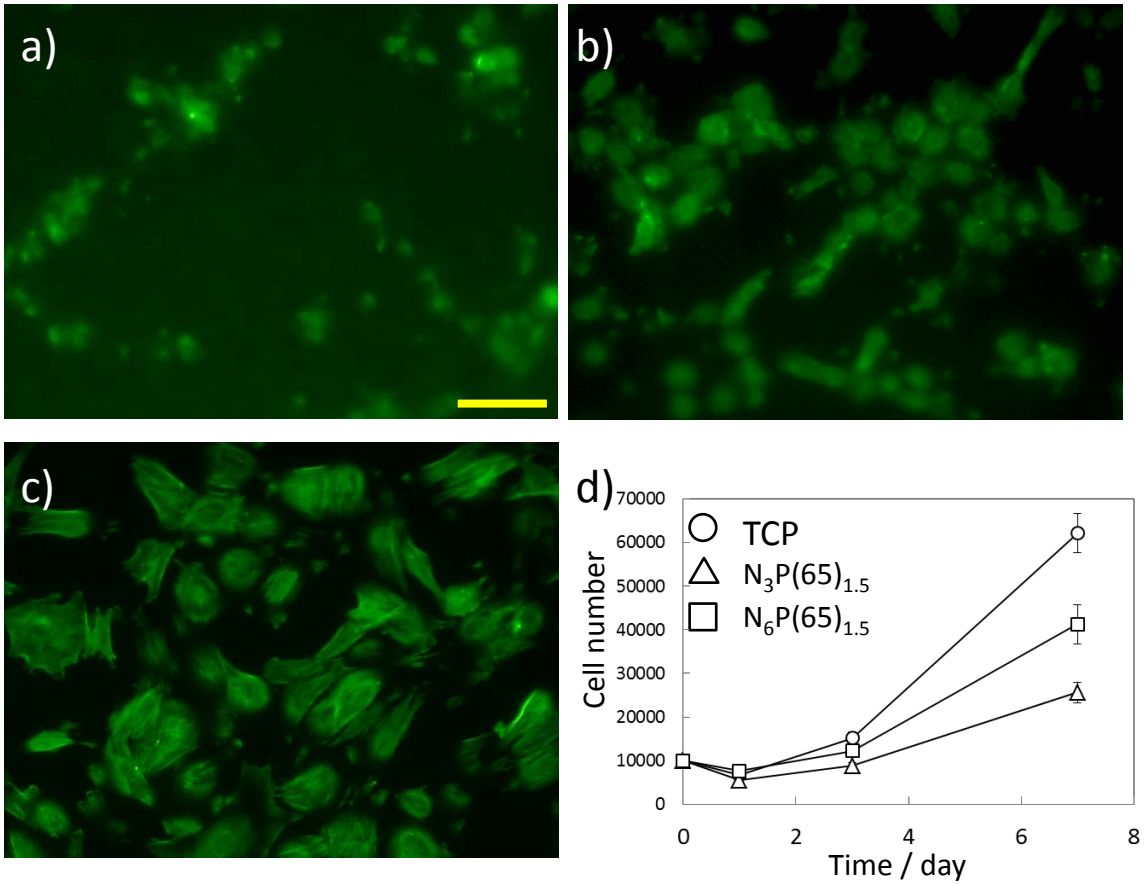

Figure 11 MC3T3-E1 cell proliferation on nanocomposite hydrogels. Fluorescent microphotographs of phalloidin binding to F-actin of cells cultured on a) $N_3P(65)_{1.5}$, b) $N_6P(65)_{1.5}$, c) tissue culture plate as a control for 7 days, and d) growth curves on these hydrogels. Scale bars represent 100 μm.

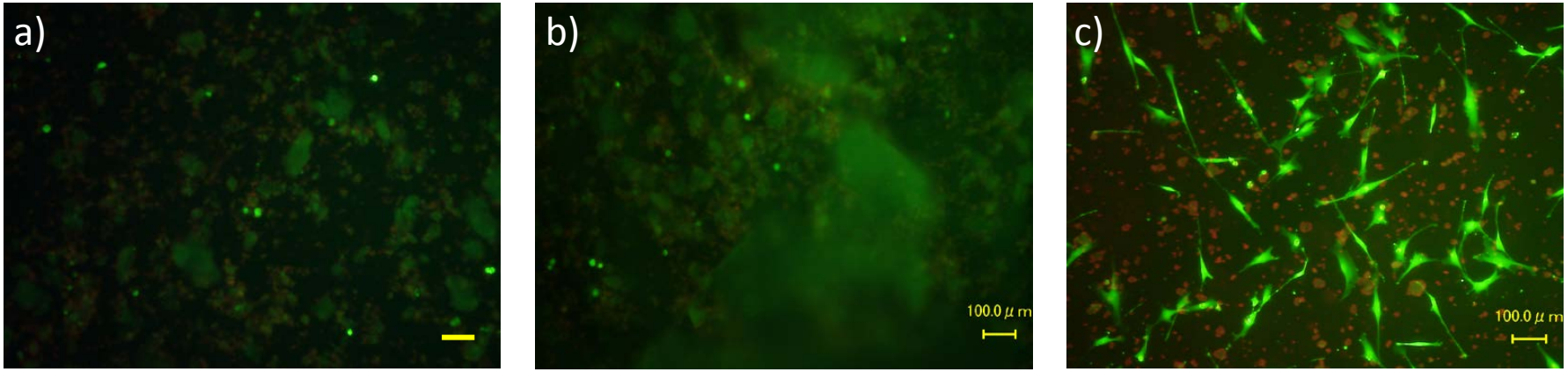

Figure 12. Cell viability of MC3T3-E1 cells after a) 24 and b) 72 hours in the nanocomposite $N_6P(65)_{1.5}$. Almost all cells were alive. c) Cells at 24 hours after seeding for encapsulation in the nanocomposite hydrogel. Scale bars represent 100 μm. Almost all cells were alive. Scale bars represent 100 μm.

Supplementary Information

Thixotropic injectable hydrogel using a polyampholyte and nanosilicate prepared directly after cryopreservation

Minkle Jain, Kazuaki Matsumura*

School of Materials Science, Japan Advanced Institute of Science and Technology, 1-1 Asahidai, Nomi, Ishikawa 923-1292, Japan

*To whom correspondence should be addressed:

Kazuaki Matsumura

E-mail: mkazuaki@jaist.ac.jp
Tel: +81-761-51-1680
Fax: +81-761-51-1149

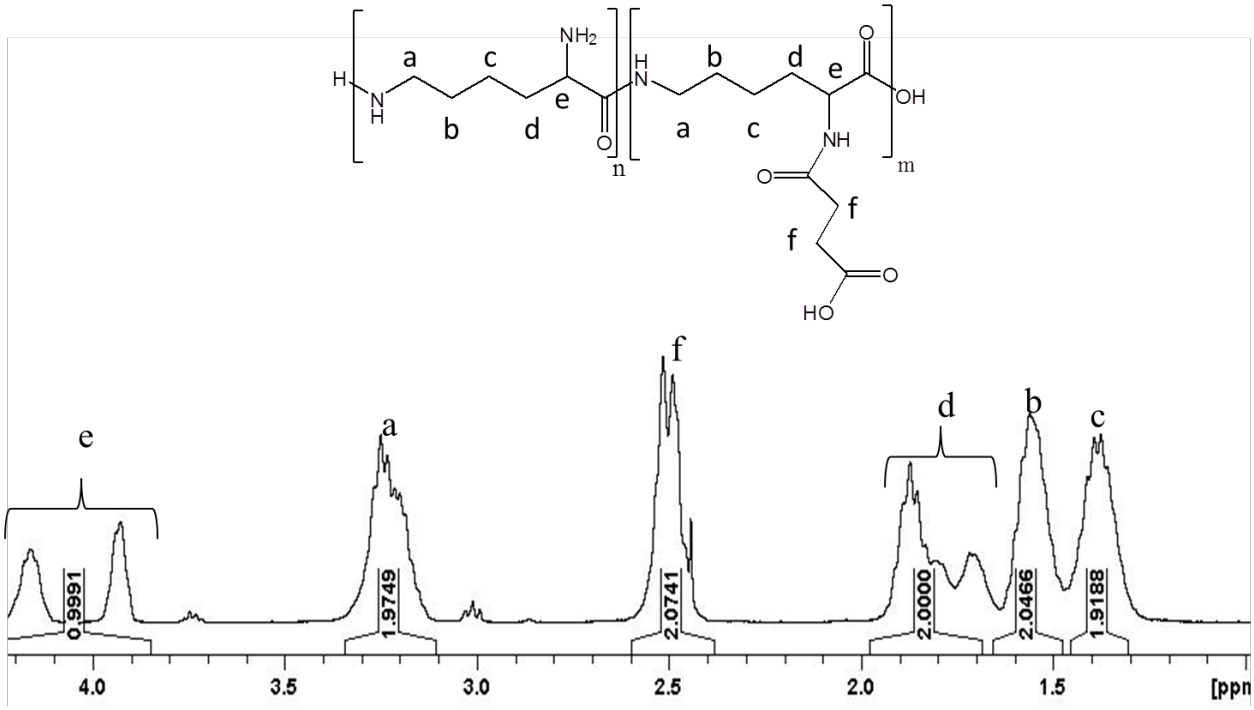

Fig. S1 ^{1}H NMR spectra of PLL (0.5)

Degree of substitution is 50%

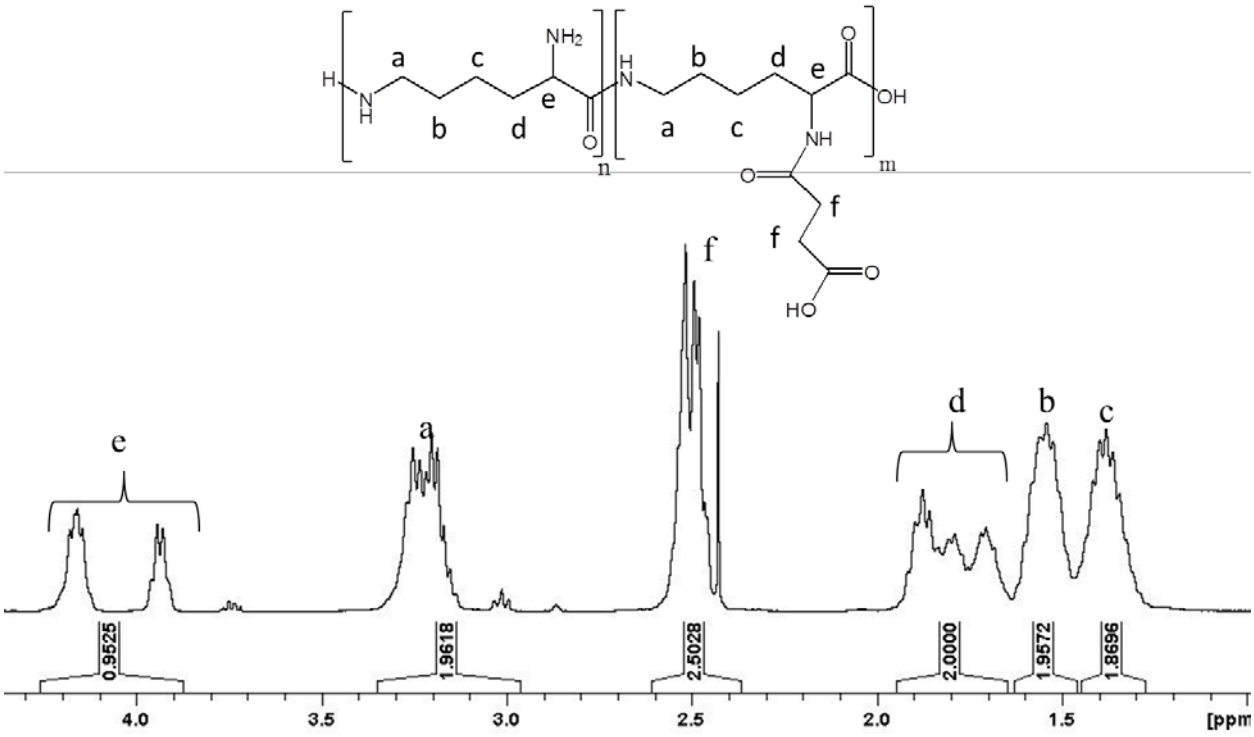

Fig. S2 ^{1}H NMR spectra of PLL (0.65)

Degree of substitution is 63%

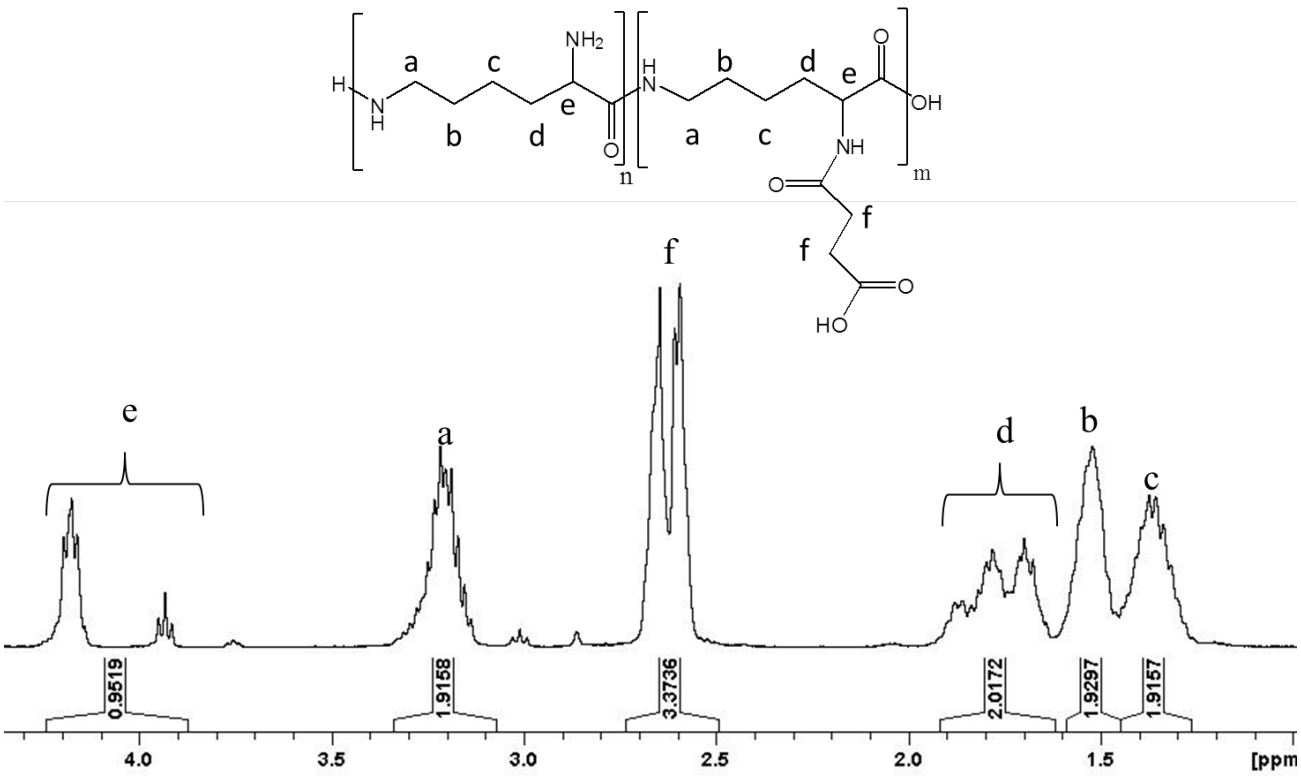

Fig. S3 ^{1}H NMR spectra of PLL (0.9)

Degree of substitution is 85%

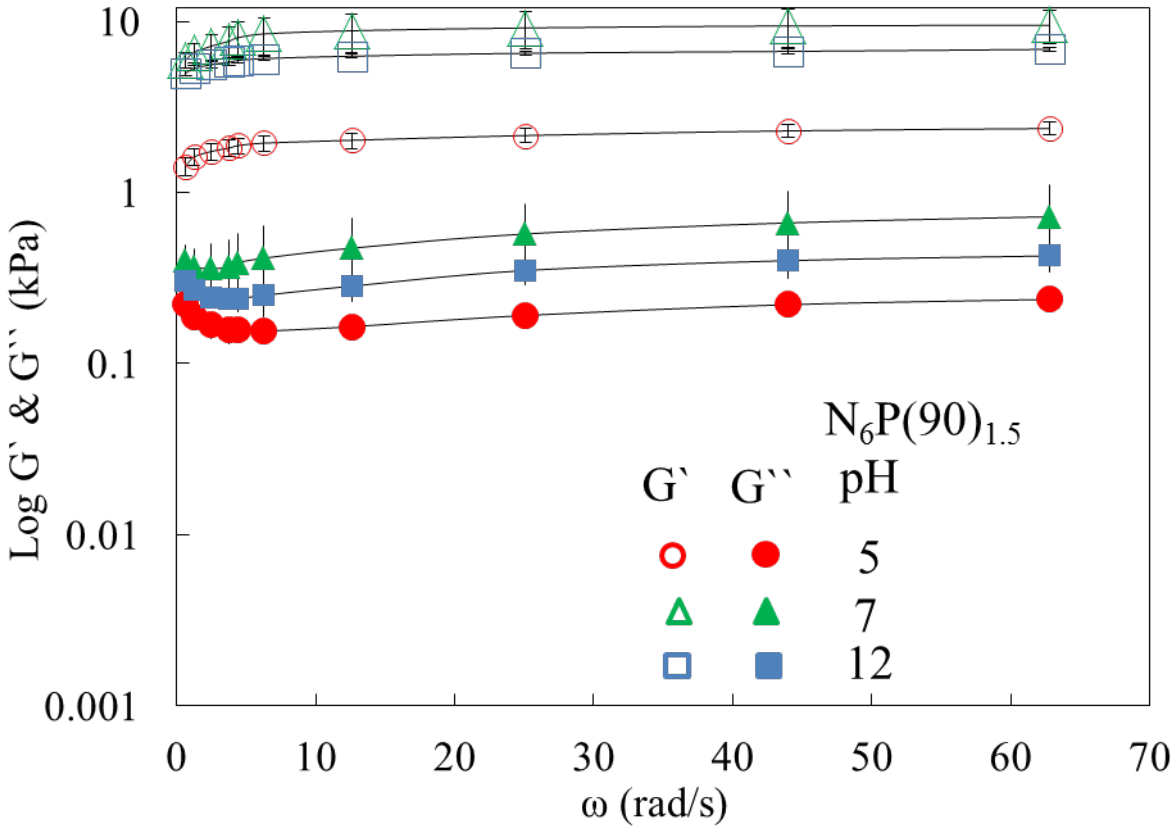

Fig. S4 Storage and loss moduli of nanocomposite N6P(90)1.5 at various pH, 37 ˚C composed of PLL (0.9).

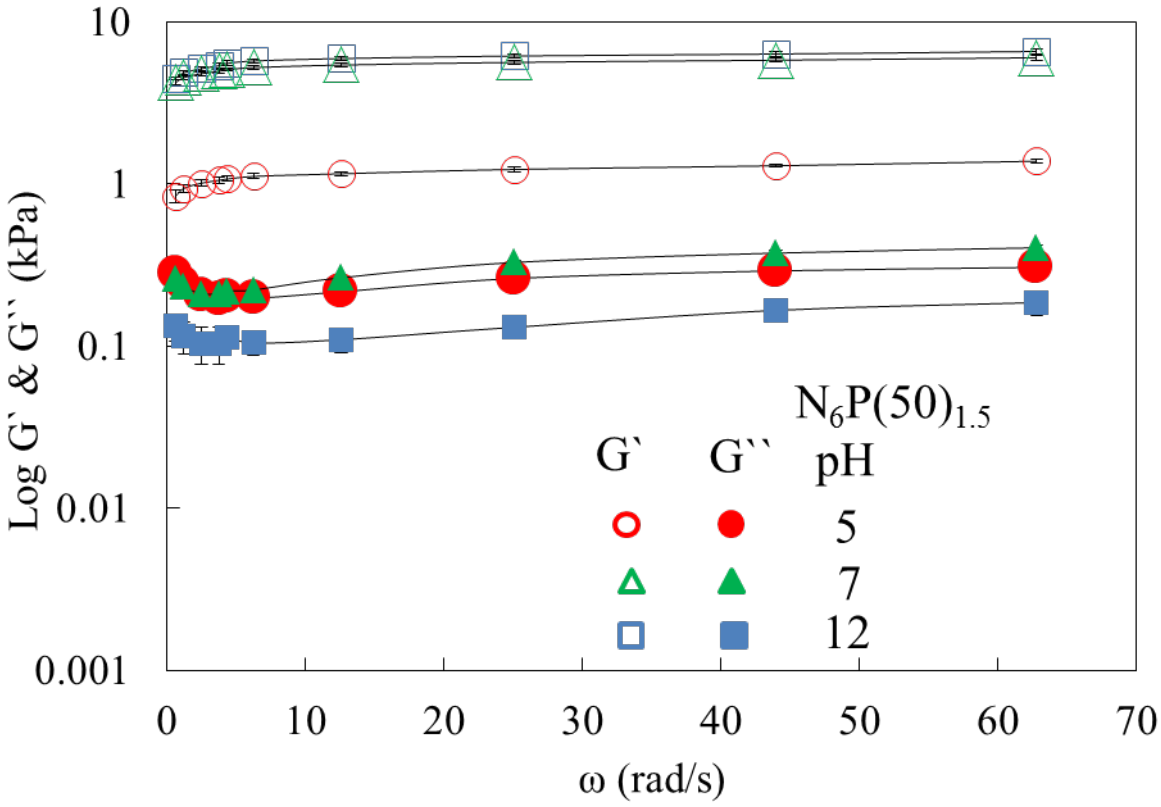

Fig. S5 Storage and loss moduli of nanocomposite N6P(50)1.5 at various pH, 37 ˚C composed of PLL (0.5).